Final report

1. Project details

Project title	EUDP 2020-II Future heat pump for small and medium sized district heating using CO_2 and mixtures as refrigerant (CO2MIX4Heat)
File no.	**64020-2037**
Name of the funding scheme	EUDP
Project managing company / institution	Danish Technological Institute
CVR number (central business register)	DK 5697 6116
Project partners	Aarhus University Fenagy Danfoss Güntner Vahterus Danish District Heating Association
Submission date	24 October 2024

2. Summary

English version:

The purpose of this project was to help small and medium sized district heating companies in obtaining their goals of establishing CO_2 neutral heat production by using energy efficient technology. The task of converting the district heating sector to a more sustainable heat production is huge, and the time frame is short. To meet these challenges, two heat pump solutions were developed in the project – both using natural refrigerants.

The first solution developed in the project is a super-efficient and price competitive, dedicated CO_2 heat pump with air as heat source. This heat pump is a factory built and mass-produced plug and play solution that can be produced in the numbers needed to cover the district heating transition in the short time frame they operate with. The heat pump uses non-toxic and environmentally friendly CO_2 as refrigerant. Simplicity is in focus to drive the price down and lower maintenance, however, without compromising the efficiency. This was accomplished by optimizing both the individual components included in the heat pump, the refrigerant cycle that the components are a part of, and the control system that is used to control the heat pump.

Measurements have shown that the efficiency of the heat pump can match up with the competing technologies when the specific properties that the CO_2 refrigerant has are utilized. At the same time, the price tag is considerably lower, the environmental concerns none, the footprint significantly smaller, and the on-site installation time is a fraction of the installation time for site-built heat pumps.

The second solution that was developed was the hydrocarbon heat pump to be used as a mechanical subcooling for the CO_2 heat pump where the return temperature from the district heating is higher than 50°C. In this way, the combination of CO_2 and hydrocarbons was made without mixing the refrigerants as originally planned. With the mechanical subcooling, the COP of the unit could be increased by 25% for the return/supply of 50/60°C.

Danish version:

Projektets formål er at hjælpe små og mellemstore fjernvarmeselskaber med at nå deres mål om at etablere CO_2-neutral varmeproduktion i den nærmeste fremtid med energieffektiv teknologi. Opgaven med at omdanne fjernvarmesektoren til en mere bæredygtig produktion er enorm, og tidsrammen er kort. For at imødekomme disse udfordringer er der udviklet to varmepumpeløsninger i projektet – begge ved hjælp af naturlige kølemidler.

Den første løsning er en supereffektiv og priskonkurrencedygtig, dedikeret CO_2-varmepumpe med luft som varmekilde. Denne varmepumpe er en fabriksbygget og masseproduceret "plug and play"-løsning, der kan produceres i det antal, der er nødvendigt for at dække fjernvarmebehovet i den korte tidsramme, der opereres med. Varmepumpen bruger ikke-giftig og miljøvenlig CO_2 som kølemiddel. En enkel systemopbygning har været i fokus for at sænke prisen og vedligeholdelsesomkostningerne – dog uden at gå på kompromis med effektiviteten. Dette er opnået ved at optimere både de enkelte komponenter, som varmepumpen består af, kølemiddelkredsløbet, som komponenterne er en del af, og det styresystem, der bruges til at styre varmepumpen.

Målinger har vist, at varmepumpens effektivitet kan blive den samme eller bedre end for konventionelle varmepumper, hvis de specifikke egenskaber, som CO_2-kølemidlet har, udnyttes. Samtidig er prisen betydeligt lavere, miljøpåvirkningerne er lig nul, fodaftrykket er betydeligt mindre, og installationstiden på stedet er en brøkdel af, hvad den er for anlægsbyggede ammoniakvarmepumper.

Den anden løsning, der er udviklet, er en såkaldt mekanisk underkøling til CO_2-systemer. Dette er en varmepumpe med kulbrinte-kølemiddel, som underkøler CO_2-kølemidlet direkte eller indirekte. Derved kan effektiviteten for varmepumpen øges ved høje returtemperaturer fra fjernvarmen. En simuleret beregning viste en 25 % øget COP for en løsning, hvor fremløbstemperaturen er 60 °C, og returtemperaturen fra fjernvarmen er 50 °C.

3. Project objectives

The objective of the project was to develop an efficient, price competitive, compact, easy to install and service friendly heat pump with a lower heat production price and with nontoxic refrigerant optimized for district heating purposes and with air as a heat source. CO_2 comprises special properties, which are well-suited for heat production at temperatures up to and above 80°C as well as lower temperatures with a considerable temperature glide on the warm side (district heating). The special properties of CO_2 have shown to increase the

energy efficiency of district heating heat pumps, which has previously not been used for district heating. Furthermore, the developed heat pump can have a great potential for efficient heat pumps in the industrial sector, where waste/surplus heat can be reused to a greater extent in the future.

The developed technology in the project has been a CO_2 heat pump with air as a heat source. To make this happen, several of the components that the heat pump composes of have been developed. These components are among others large size valves for 140 bars needed for further development of CO_2 heat pumps. These valves were designed by Danfoss. Ejectors for industrial heat pumps were developed by Fenagy. A new evaporator design was designed by Guentner which included both a v-coil air cooled evaporator and flat bed.

A concept of mechanical subcooling has been developed, built, and tested in the project. This concept is to increase the efficiency of CO_2 heat pumps where the return temperature of the district heating water is above 45°C. This concept showed considerable energy efficiency improvements and moved the CO_2 heat pumps as a competitive solution for the higher return temperatures.

4. Project implementation

Changes were made during the project when it became clear that having both a CO_2 heat pump and a heat pump with mixtures was too extensive for one project. Permission was given by the EUDP to exchange the mixture part of the project with a concept of mechanical subcooling. Here, the isobutane heat pump was designed to subcool the return water of the district heating to improve efficiency. Apart from that, the project proceeded according to the original plan.

The project started by assembling knowledge in WP01 before the system design was made in WP02.

In WP02 Research on new system design: The CO_2 system design was made, and the components were developed. A master's thesis was made at Arhus University where various cycle configurations were simulated.

The frosting and defrosting of the CO_2 heat pump was investigated. A model was made of the heat pump, of the frosting process, of the finned tube heat transfer and of the air circulation around the source evaporators. This model was used to predict the most efficient defrosting cycle.

Simulations of seven cycle layouts were done to be able to select the right cycle configuration.

In cooperation with Danfoss, a Bachelor Thesis was done working on modelling of transcritical CO2 heat pumps including ejectors and expanders.

Several defrosting methods were established, and then eight were selected to be simulated.

In the mixture part of the project, a master study regarding using mixtures as a refrigerant was made at Arhus University. These showed great potential when the glide on the hot and cold side was greater than 20K.

The mechanical subcooling concept was investigated, and promising simulations were done. This led to a design of a unit to be used as a mechanical subccoler.

In WP03 CO_2 control systems and communication with SCADA: The control system of the heat pump was developed. The control strategies and the control loops were identified. The findings were built into PLC software by Fenagy and integrated into the electrical cabin. This was done for both the test unit installed at DTI and the field test unit installed at Harlev District Heating.

In WP04 Customization and commercial targets: The customer needs were investigated and integrated into the heat pump design to ensure a product that the customer demanded. This work package was divided into two main focus areas, i.e. customization and commercial targets.

In the customization of the heat pump design, the focus was on a compact factory-built unit, which was factory tested, plug-and-play and ready to be installed at the customer.

The design took into consideration both installation and service friendliness. This was done to reduce the price for installation and to ease the service.

The heat pump control system was developed to integrate easily into the surveillance systems used by the district heating company.

The commercial targets that were addressed were done to ensure the success of the product and to ensure broad customer acceptance. Focus was on lowering the price as much as possible without compromising the efficiency and, thereby, the longer-term profit.

The focus was also on a smaller footprint, but without compromising the service friendliness.

In WP05 Functional analyzes: Here, the functional analyses were done. A 100 kW CO_2 test heat pump was developed and installed in a climate chamber at the DTI laboratory in Aarhus. Detailed measurements were done in a simulated real-life situation. A data analysis was performed, and a part of the analysis was to verify the simulation tools made in WP02 against measurements. 27 tests were performed to investigate the icing of the evaporator and the following defrosting, the capacity of the heat pump and the COP, the liquid distribution in the coil etc.

Based on the results of the 100kW CO_2 test heat pump, an actual size of 300kW was designed and built. This heat pump was installed in ambient conditions and attached to a test setup at DTI in Aarhus. Tests were performed to measure the capacity and the COP, the ice buildup and defrosting, and the air distribution.

For the mechanical subcooling, an isobutane unit was built, installed, and tested at DTI. The simulations were verified.

Danfoss' development of 140bars valves in the project was tested and verified. A specific test rig was built to perform these tests.

In WP06 Functional analyzes of CO_2 system at district heating site: A heat pump was installed at Herlev District Heating for field test. Measurements on the running conditions under real-life situations were made.

In WP07 Dissemination: The part of the project was presented both in articles, on conferences, and on theme days.

An article was written in the International Journal of Refrigeration in 2022 about the use of mixtures in heat pumps.

A presentation of the project was done on a theme day held at Dansk Fjernvarme in 2022. The focus was on defrosting evaporators.

In 2023, a presentation was made on the 8th international symposium on Advances in Refrigeration and Heat Pump Technology conference in Denmark around defrosting in CO_2 heat pumps and the use of mechanical subcooling to boost the efficiency of CO_2 heat pumps for high return temperatures.

A paper was written and presented at the IIR2023 in Macedonia around defrosting in CO_2 heat pumps. Another paper was written and presented at the ICR2023 conference in Paris around mechanical subcooling.

According to the application, Danfoss should design and develop the ejectors but as the project developed, they did not have resources to engage in this, so the ejector development was taken over by Fenagy, and they developed the ejectors in the project.

In the application, one of the tasks for Danfoss was to develop a control platform for CO_2 heat pumps together with Fenagy. It turned out to be impossible to do this joint development, and Fenagy ended up doing the control of the heat pump without Danfoss.

The milestones of the project were met for the CO_2 heat pump part. For the mixture part, the milestones were changed from the original application. The described dissemination milestones were met. However, the results were not presented at the specific conferences mentioned in the application as the dates for these conferences turned out to be too early in the project to be able to present results.

The biggest problem that was experienced was the mal distribution of liquid refrigerant in the air evaporator coil. A lot of tests were conducted to find a solution to this problem. The problem is complicated since it can come from both the refrigerant side and the air side. The solution to that problem was to develop and install adjustable air hoods to even out the air flow mal distribution.

Another issue that was not expected was the defrosting of the evaporators that required a lot of attention. It turned out that it was hard to get an even distribution of the refrigerant through the coil during defrost.

5. Project results

The original objective of the project was to develop an air to water heat pump for the district heating sector with good efficiency, a competitive price and a small footprint. Another objective of the project was to develop a heat pump with mixtures as a refrigerant.

The focus areas in the project were five. The first one was to design a refrigeration cycle using CO_2 as a refrigerant. Another focus area was to design a heat pump using mixtures of CO_2 and other natural refrigerants. The third focus area was directed at the air evaporators for the heat pump. The fourth focus area was on customization where the focus was on designing factory-built units with natural refrigerant CO_2 that were easy to install and service and designed for the district heating. The fifth focus area was to design a unit with a low price, a small footprint, using natural refrigerant, with a low heat production price and used in the district heating.

There were two tracks in the project. The first was the CO_2 heat pump including a new rack design and evaporators. This track included design and optimization of compressor technology, ejectors, refrigeration cycle, and control system. For the evaporators, the superheat out of the evaporator was in focus as well as the evaporator coil design, the circuit optimization, and the defrost strategies.

In the second track regarding mixtures, the initial intention was to develop a heat pump with refrigeration mixtures for the heat pump application with a temperature glide on the source and sink side. The initial investigations were done, and it was evaluated that the task of designing the concept, and the needed equipment was too large a task together with developing the CO_2 heat pump. Thereby a shift was made in the mixture part of the project to develop a mechanical subcooling concept instead of the initial mixture part. Here an isobutane heat pump cycle is used to bring the high return temperature from the district heating down to lower heat which is beneficial for the CO_2 heat pump and raises the overall COP of the unit.

To develop the heat pump concept in the project, the work was divided into five work packages.

5.1 Research on new system design WP02

For the first track, some components had to be developed to be able to fulfill the system requirements. This was done in WP02. This included a new high-pressure valve developed by Danfoss. A test stand was built where the valves were tested for pressure drop and functionality. This test rig can be seen in the PI diagram in Figure 2. The valves were integrated in the test heat pump for a longer time testing, see Figure 1.

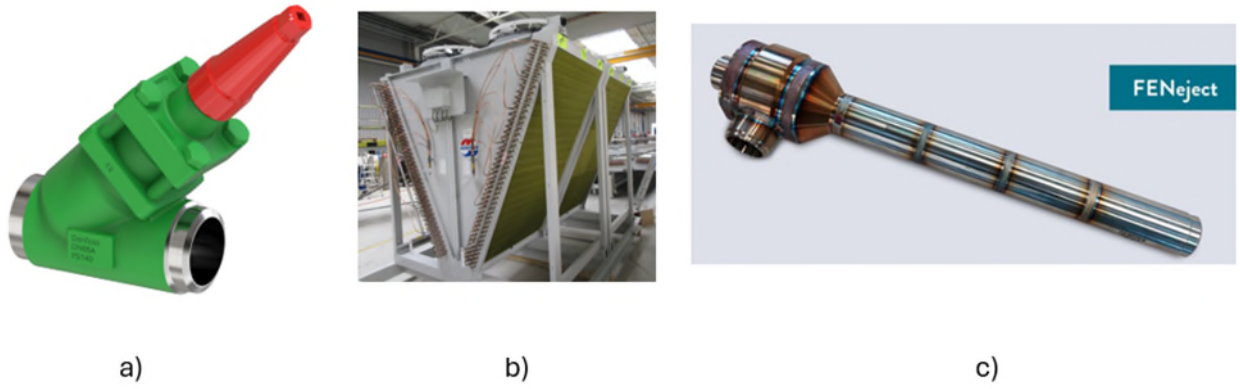

Figure 1: Components developed in the project. a) High pressure valves from Danfoss, b) Air evaporator from Guentner, c) Ejector from Fenagy.

Another component was a V-Coil air evaporator that needed to be designed to be able to reduce the footprint of the total heat pump solution. The evaporator in the test unit had four evaporator coils where each had a different pipe configuration to test what would be the best configuration.

Another energy enhancing component to be developed in the project was ejectors. These were developed by Fenagy in the project. The ejector can be seen in Figure 1.

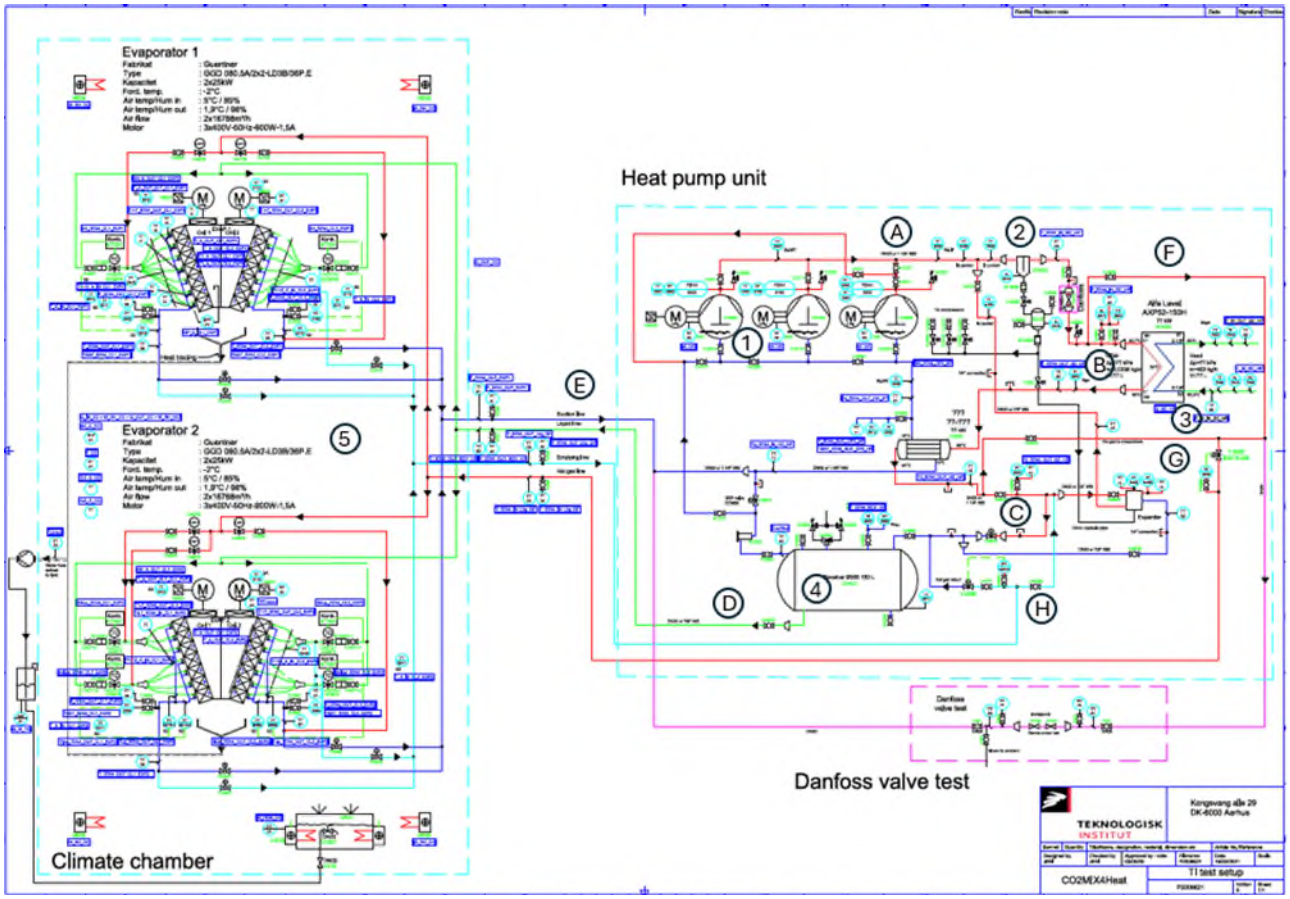

Figure 2: PI diagram of the test heat pump.

The test setup was designed in WP02 and built according to Figure 2. The heat pump has three compressors where one is with frequency drive. The test setup has several options. It can run as a normal MT compressor, as a parallel compression cycle, and as a booster system. The evaporator is placed inside the climate chamber where temperature and humidity can be controlled. The heat pump compressor part is placed outside the climate chamber.

The goal of the research activity is two-fold: (1) to develop models for prediction of frost and de-frost time and pattern on multi-circuit air-source evaporators, (2) to specifically study the frost pattern on V-shape evaporators used in the developed systems.

To start with, a lot of simulations were done in the research part of the project. The research part evolved around a:

- CO_2 refrigeration cycle design
- Frosting of the evaporator
- Defrost strategies
- Evaporator air circulation
- Mixtures
- CFD solver for two-phase ejectors.

5.1.1 CO_2 refrigeration cycle design

In the compressor refrigeration cycle part, the following seven configurations were investigated:

1. Basic MT system
2. Parallel compressor
3. Parallel compressor with HP Ejector
4. LP Ejector
5. MT cycle with expander
6. Parallel compressor with expander
7. Booster configuration.

All these configurations were integrated into the design of the test setup. The reference cycle was the basic MT cycle shown in Figure 3. The basic MT cycle is adjusted by closing the valves A, B, C, D, and E. Thereby, all compressors suck from the evaporators through the suction gas heat exchanger. When shifting to a parallel compressor system, the valves A and D are opened, and the valves G and F are closed. In this way, the first compressor acts as an IT compressor sucking from the receiver while the two other compressors suck from the evaporators. For the third combination, the HP ejector is put into operation by opening valve C. The ejector then sucks from the suction line and delivers to the receiver where the parallel compressor compresses it up to the gas cooler pressure and thereby reduces the work on the MT compressors. The fourth combination is accomplished by opening valve G and closing valve H and I. Here all the compressors suck from the receiver, and the ejector works as an LP ejector sucking the gas from the evaporators and delivering it to the receiver. For the fifth combination, the valves H, I, F, and E are opened, and the valves A, C, and D are closed. Here the expander is working as a parallel compressor, using the expansion energy to lift the flash gas up to the gas cooler. For the sixth combination, both the expander and the parallel compressor are used. Here the valves G and F are closed, and the valves A and D are open. Now the first compressor acts as a parallel compressor compressing the flash gas from the receiver together with the expander. For the last configuration where the heat pump is running as a booster system i.e., one compressor delivers the gas to the next one to compress it further. Here the valves B, G, K, and I are opened, and the valves A, I, J, and L are closed. In this way, the last compressor discharge gas is mixed with the flash gas coming from the receiver before entering the first two compressors.

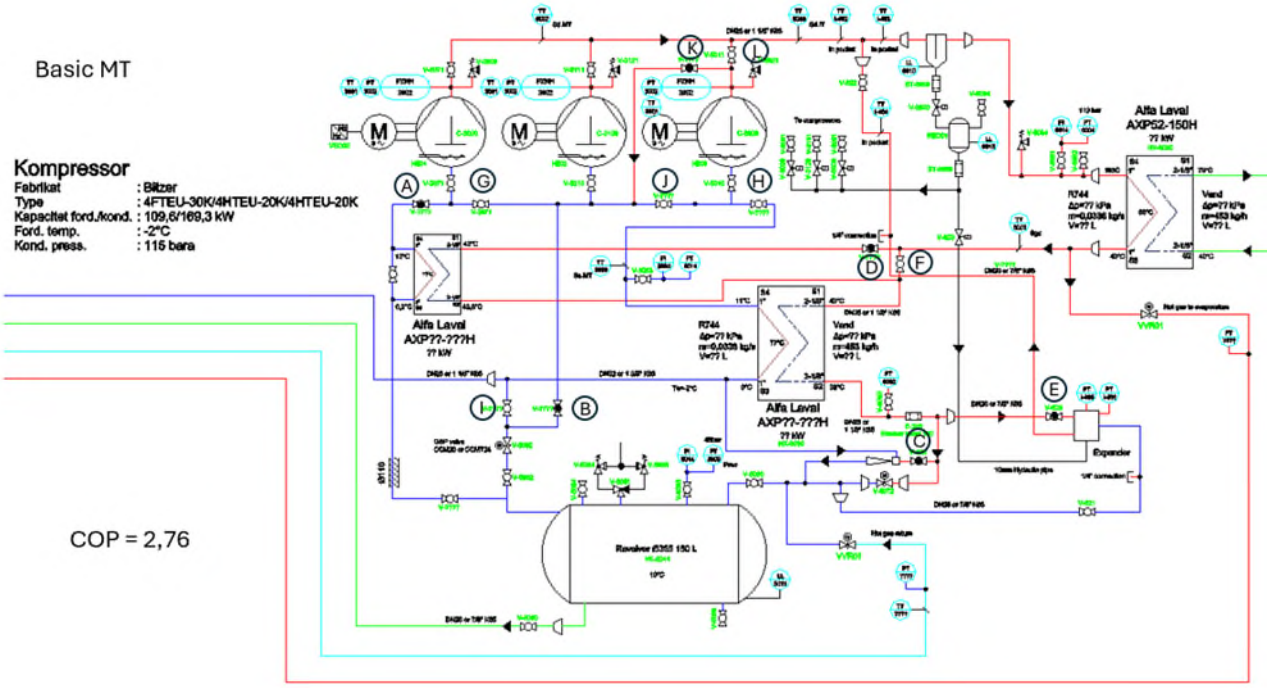

Figure 3: The reference system – a basic MT system.

To compare the solutions, simulations were made using a model built in EES. The comparison is made on the COP of the seven configurations as seen in Table 1.

The assumption used in the calculation was a district heating temperature set of 70°C from the heat pump and returning at 40°C to the heat pump. The pinch point in the heat exchangers was set as 2K. The inlet air temperature to the evaporators was set to 5°C with a humidity of 85%. The air leaving the evaporator was 1.9°C and with a humidity of 98%. This resulted in an evaporation temperature of -2°C and superheat of 2K.

Table 1: COP values for the investigated cycle solutions

Solution	COP	% improvements
1. Basic MT system	2.76	0.0
2. Parallel compressor	3.03	9.8
3. Parallel compressor with HP Ejector	3.16	14.5
4. LP Ejector	2.97	7.6
5. MT cycle with expander	3.27	18.5
6. Parallel compressor with expander	3.38	22.5
7. Booster configuration	3.00	8.7

As seen in the table above, a 9.8% improvement in COP can be achieved by using a parallel compressor configuration. The best COP is found by utilizing the expansion energy i.e., by using an HP ejector or expander. Especially by using the expander. To utilize this, a development within the expander must be done. The booster system configuration is also interesting when looking at the improvements in COP since it is a relatively simple system configuration. The booster compressor will have a low-pressure lift and is on the edge of its running limit diagram. To be able to use this system configuration, a new compressor type must be developed.

5.1.2 Frosting of the evaporator

5.1.2.1 Introduction

In cold climates, air source heat pumps (ASHP) face the challenge of frost formation on outdoor evaporators, which can be addressed by periodic defrosting. However, a well-known factor that causes inefficient defrosting and adversely affects the performance of an evaporator is an uneven frost formation with a non-uniform air flow distribution playing a major role. This part focuses on details of uneven frost formation due to non-uniform air flow distribution in the outdoor V-shape heat exchangers of an air source CO_2 heat pump, due to the complex geometry of V-shape multi-circuit heat exchangers, the air flow distribution is non-uniform among the circuits, leading to a variation in the frost growth rate.

5.1.2.2 Frost model

5.1.2.2.1 Model description

Since the frost model and its results are published as a journal paper, the present report only features a brief description. A computational fluid dynamic (CFD) assisted evaporator model is developed in which, at each time step, the airflow distribution among the circuits is determined by means of a CFD simulation and used as an input to the frosted evaporator model. Figure 4 represents the simulation algorithm.

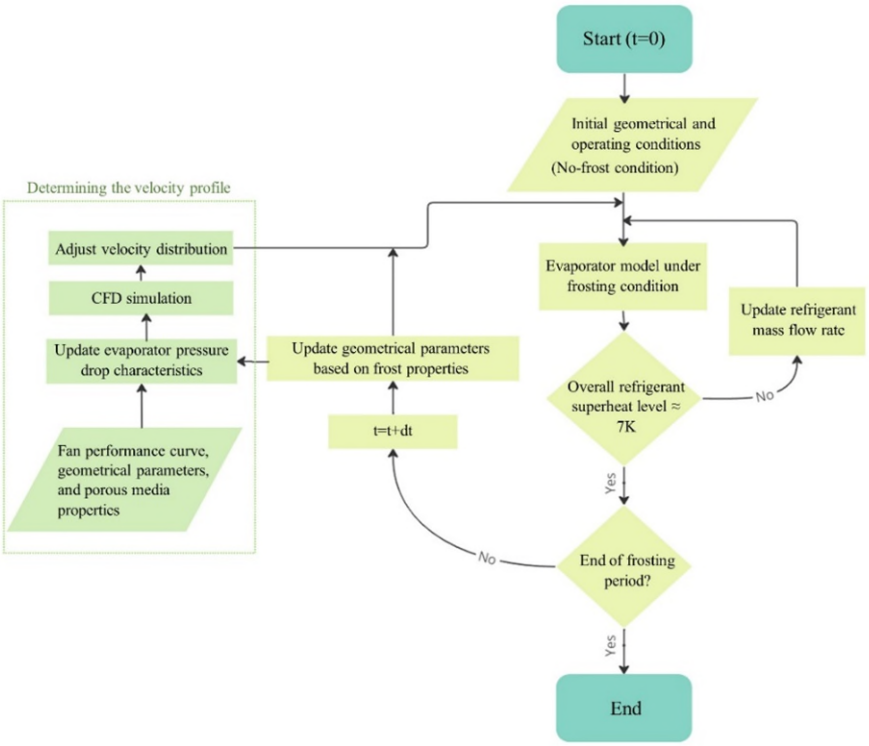

Figure 4: Algorithm for the model of the multi circuit evaporator under frost conditions.

Under different frosting conditions, we analyze the local frost accumulation on the evaporator surface. As well as demonstrating that a non-uniform airflow distribution causes non-uniform frost formation, the results also show that the non-uniform frost formation causes the air flow distribution among the circuits to change over time, and the rate at which this change occurs depends on the ambient conditions.

5.1.2.2.2 Study of a V-shape evaporator

The developed heat pump solution in the CO2MIX4Heat project relies on V-shape evaporators provided by the project partner Guntner, whose frost formation behaviour is studied here. The studied evaporator is a V-

shape type having four separated units, and each unit has seven refrigerant circuits. A schematic for the V-shape evaporator and the details of the refrigerant circuits are shown in Figure 5.

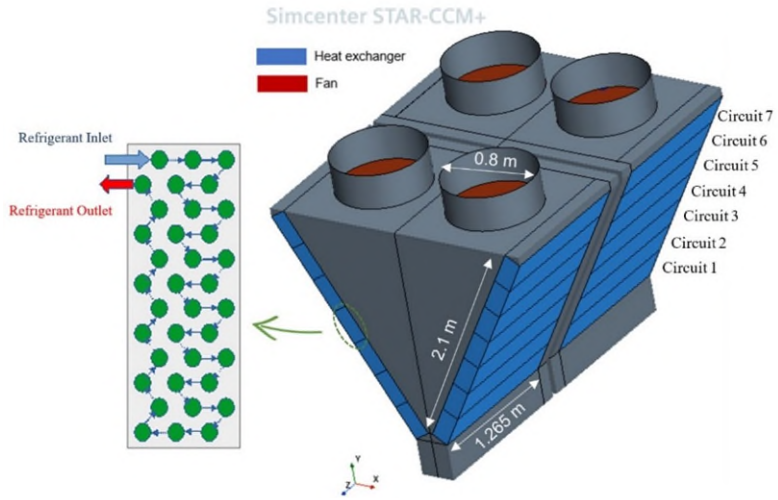

Figure 5: Schematic of the V-shape evaporator and the details of the refrigerant circuits.

The different cases studied in this report are shown in Table 2. The objective of this study is to investigate the effect of environmental conditions on frosted V-shape evaporator behavior. Therefore, the problem is solved under three different conditions.

Table 2: The studied cases of frost formation.

	Ambient temperature	Relative humidity
Case I	2°C	50%
Case II	2°C	70%
Case III	2°C	85%

5.1.2.2.3 Results and discussion

The total frost mass accumulated on the seven circuits after one hour are displayed in Figure 6. The cases II and III with a relative humidity of 70 and 85% follow the same trend: the first two circuits with lower air mass flow rates show the lower amount of accumulated frost, and the frost weights in other circuits are relatively similar. However, Case I with a 50% air relative humidity shows a different trend, and the accumulated frost in the second circuits is the highest. This difference in behaviour can be explained by looking at the effects of two parameters, namely the air flow rate and the air dew point temperature.

It must be kept in mind that surface temperatures below air dew point and freezing point result in air moisture freezing. The dew point temperatures are -7.3, -2.9 and -0.3°C in the cases I, II and III, respectively. An increase in air flow leads to a higher condensation rate as well as a higher heat transfer rate, which results in a higher evaporator surface temperature in tubes containing superheated gas. In case III, all surface temperatures are below the dew point temperature after one hour, while in case II, only one tube element of the three upper circuits has a surface temperature above the dew point. However, as shown in Figure 7, in case I, a large part of the upper circuits has a surface temperature above the dew point (-7.3 °C), and there is no condensate on these parts. Therefore, there is less frost on their surfaces since the surface temperatures are higher than the dew point.

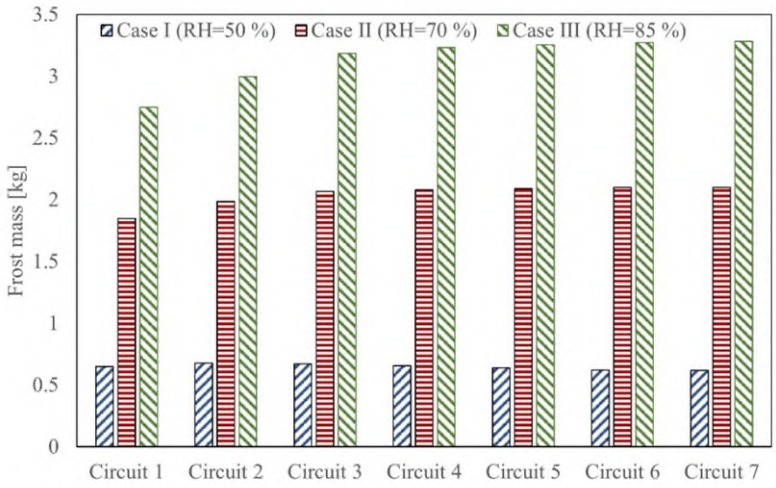

Figure 6: Frost accumulation on the circuit's surfaces after 60 minutes.

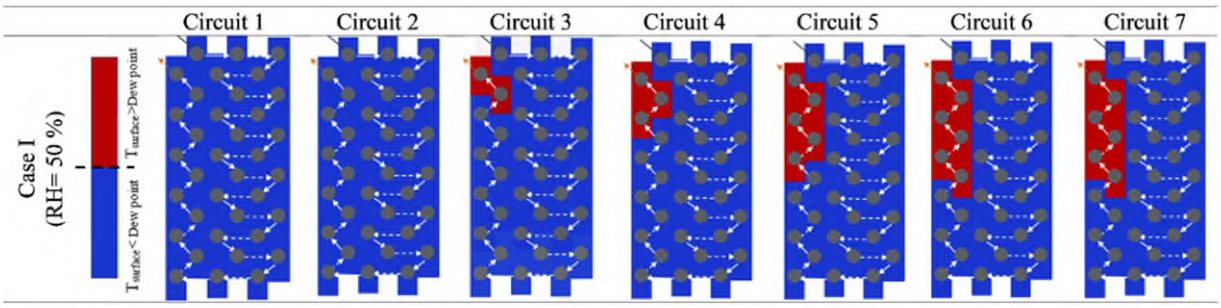

Figure 7: Comparison of the surface temperature with the dew point temperature after one hour for case I. Red shows temperature higher than dew point temperature.

To shed further light on the patterns of frost formation, Figure 8 demonstrates a detailed view of the blockage ratio on different tubes of the seven circuits for all studied cases after 60 minutes of frosting. Here, the amount of frost is indicated by the blockage ratio (BR) which is the ratio of frost thickness to half of fin spacing. It can represent the fraction of air flow passage blocked by frost accumulation. As seen in Figure 8, in operating conditions where air humidity is higher, thicker frost layers are formed due to a higher condensation rate. Comparing frost formation patterns between different circuits reveals the noticeable effect of the air flow velocity. As discussed before, a major consequence of air-flow non-uniformity is different levels of superheat at different coils, which in the present case translates to almost no superheat in the two lower circuits. Obviously, the frost thickness is directly affected by the surface temperature, and hence the superheat level. As a result, at the two lower circuits, there are always thick and relatively uniform layers of frost over the upstream rows. The thickness of frost decreases constantly in the downstream direction. In contrast, at the upper circuits, there are thinner layers of frost with a more heterogeneous pattern following the superheat pattern. Here, starting from the third-row, frost thickness increases leading to a larger overall mass of frost.

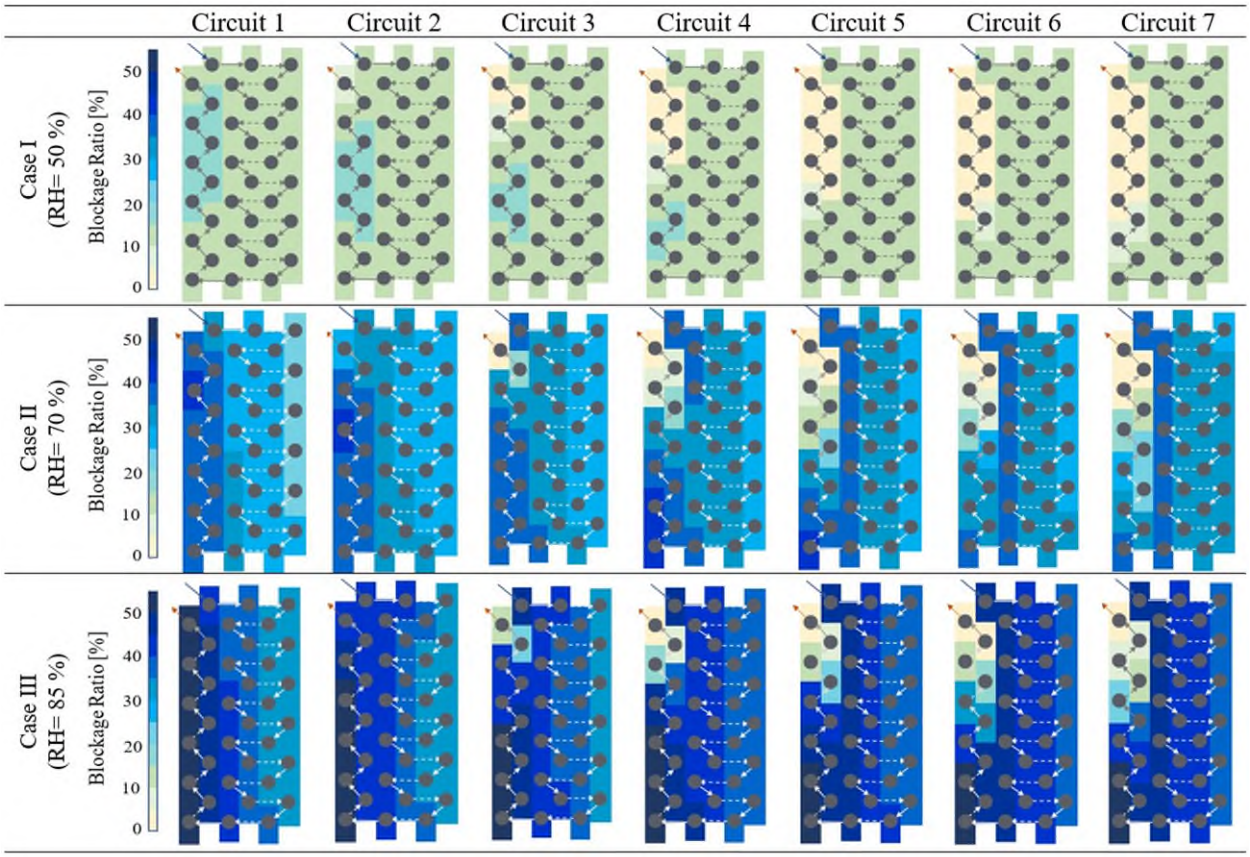

Figure 8: Blockage ratio distribution after 60 minutes.

5.1.3 Defrost strategies

As a part of WP02, an analysis of the defrost of the evaporators was made. Six possible defrost methods were investigated. The first three are shown in Figure 9 where the first one is where the defrost is done by using the high temperature high pressure gas (hot gas defrost) from the compressors before the gas cooler. The CO_2 gas can be cooled in the coil or condensed in the coil depending on the pressure that the defrost is accomplished at. The next defrost method is to take the low temperature high pressure gas (cold gas defrost) where the gas to defrost is taken after the gas cooler. The idea here was to use the CO_2 gas after it had delivered the heat to the district heating. This gas could both be used by cooling down the transcritical gas during defrost if pressure is above the critical point or by condensing the gas in the coil if the pressure is lower than the critical point. The third idea was to use the return water from the district heating to heat up a glycol circuit that then flows through separate pipes in the evaporator coil to do the defrost.

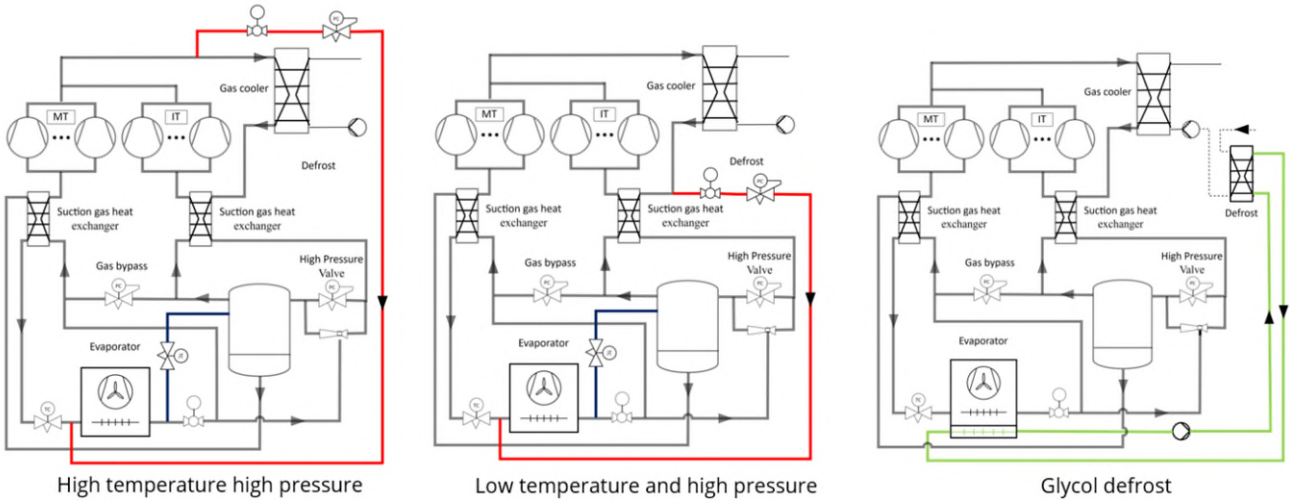

Figure 9: Investigated defrost methods.

The three other defrost methods investigated were to use a dedicated compressor to pressurize the gas from the receiver up to a pressure needed for the defrost. The next investigated defrost method was to use the energy in the liquid CO_2 refrigerant to defrost. This was done by directing the liquid through the evaporator during defrost and to melt the ice by cooling down the liquid refrigerant to the other evaporators. The next defrost method was to use the gas bypass from the receiver before the IT compressors and direct it to the evaporator during defrost. In this method, the CO_2 gas condenses in the evaporator while melting the ice, and the liquid CO_2 is collected in a vessel that is emptied by the HP ejector in the system.

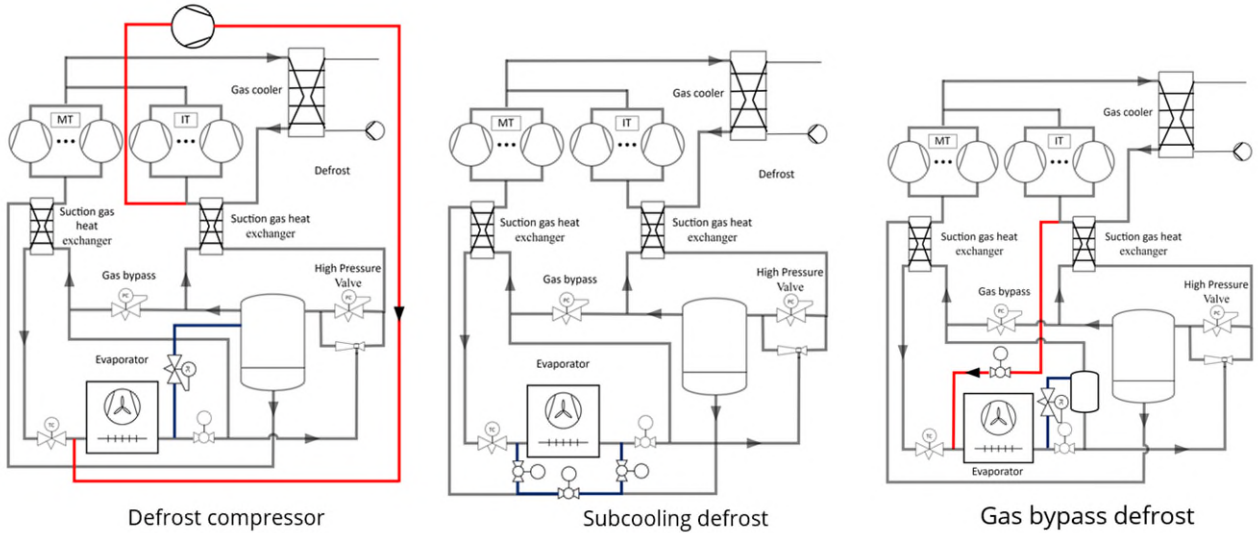

Figure 10: Defrost methods investigated.

The air conditions into the evaporator were taken as a temperature of 5°C and a humidity of 85%. Out of the evaporator, the air temperature was 1.2°C, and the humidity was 100%. The defrosting temperature where the CO_2 gas was condensed in the evaporator is considered to be minimum 5°C. The average ice thickness on the coil was set to 1mm when defrost was initiated and was estimated evenly distributed on the fin surface. The density on the ice was chosen to be 115 kg/m^3. These conditions gave 145 kg ice on the coil when the defrost started. The defrost power used was estimated to be evenly distributed for the 20 minutes it took to remove the ice and was calculated to 52 kW.

Simulations were done to investigate the reduction in COP and the capacity reduction during defrost. Two situations were investigated. One where the compressors were uncontrolled i.e., during defrost the delivered capacity reduced, and another where the compressors were controlled to increase the rotational speed to compensate for the missing capacity.

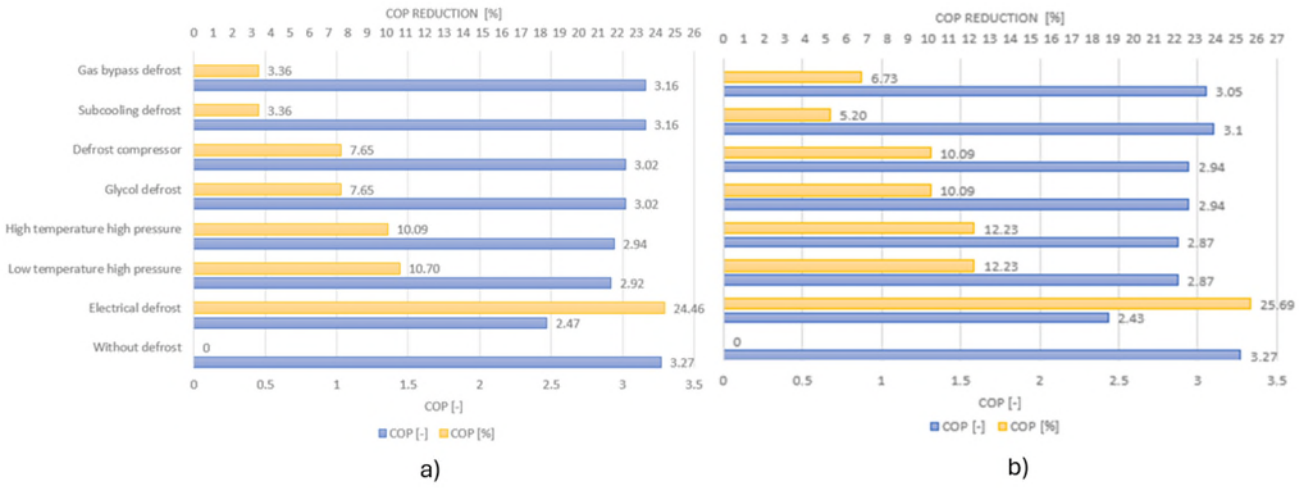

Figure 11: COP reduction for a) uncontrolled and b) controlled compressors during defrost.

The COP is depictured as the real number and the percentage drop compared to COP without defrost. The first thing to notice is that the COP reduction is larger for the case where the compressors are controlled since we need to use electrical energy to maintain the capacity. For both cases, the subcooling defrost seems to be a very good defrost method that maintains the COP best. But when doing calculations on the energy content in the subcooling, it turns out that the energy is not enough to complete the defrost in the time needed. Gas bypass defrost is good but suffers from the fact that if the air temperature is low, the receiver pressure (saturated temperature) drops, and when it comes below 5°C, the defrost is not possible. A defrost compressor is the next interesting solution, but it is complex and more expensive, and since glycol defrost has the same potential, it is a better solution. Regarding COP, the high temperature high pressure (hot gas) and low temperature high pressure (cold gas) defrost turned out to give nearly the same COP during defrost. Then the alternative is electrical defrost where electric heating rods are installed inside the coil. When defrosting the evaporator is turned off, and the electrical heating rod is turned on. This method gives the lowest COP during defrost.

Since the COP reduction is not the only parameter that defines which defrost is the best, we need to look at capacity reduction during defrost since that defines how much the production is affected during defrost. For the uncontrolled compressors during defrost, the capacity reduction is shown in Figure 12. For the controlled compressor capacity during defrost it is the same since the compressors compensate for the capacity reduction by increasing the compressor speed.

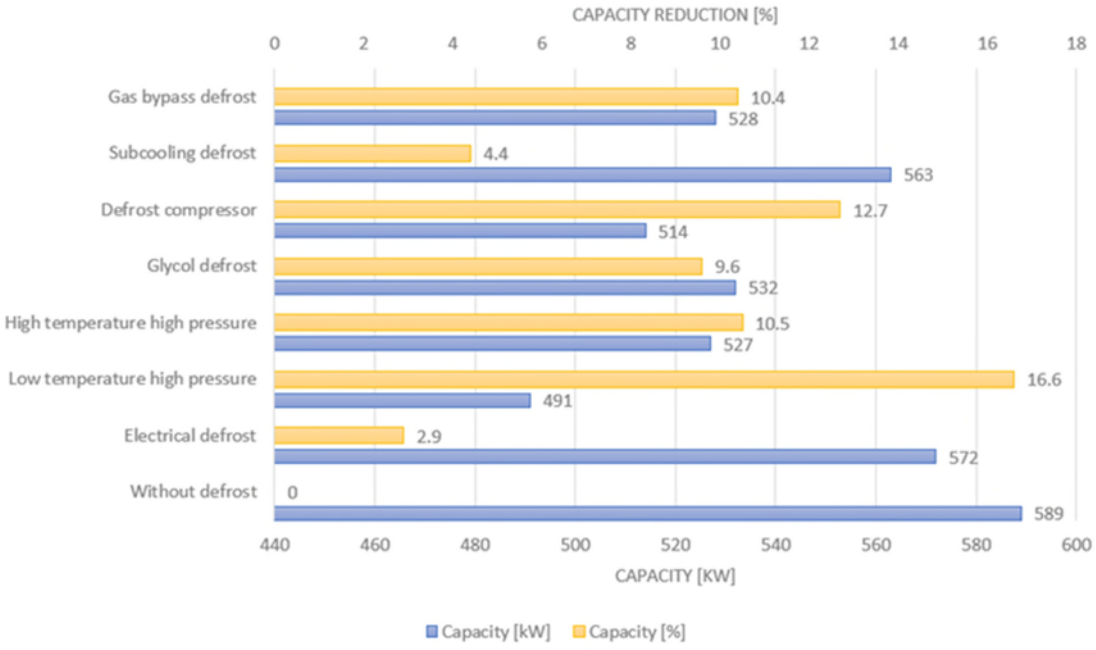

Figure 12: Capacity reduction during defrost for uncontrolled compressors.

Here the electrical defrost is the best since it has the lowest reduction in the delivered capacity of the heat pump. The low temperature high pressure (cold gas) defrost gives a large reduction in capacity because of the large mass flow to the defrost which is bypassed the ejector and into the receiver. In this way, the IT compressors are oversized and need to reduce the capacity as they would otherwise reduce the pressure in the receiver too much.

From these evaluations it is hard to evaluate which defrost is the best. When defrosting, the heat pump reduces its COP, and for the normal heat pump case, it produces less heat. The price of defrost is found by considering the drop in revenue by the reduction in produced capacity and the reduction in COP that increases the cost to produce the heating capacity. This extra cost is depictured in Figure 13 as the cost for each defrost. The electrical price was taken as 240 EUR/MWh, the price of heat as 101 EUR/MWh, and the total defrosting time was estimated to be 40 min.

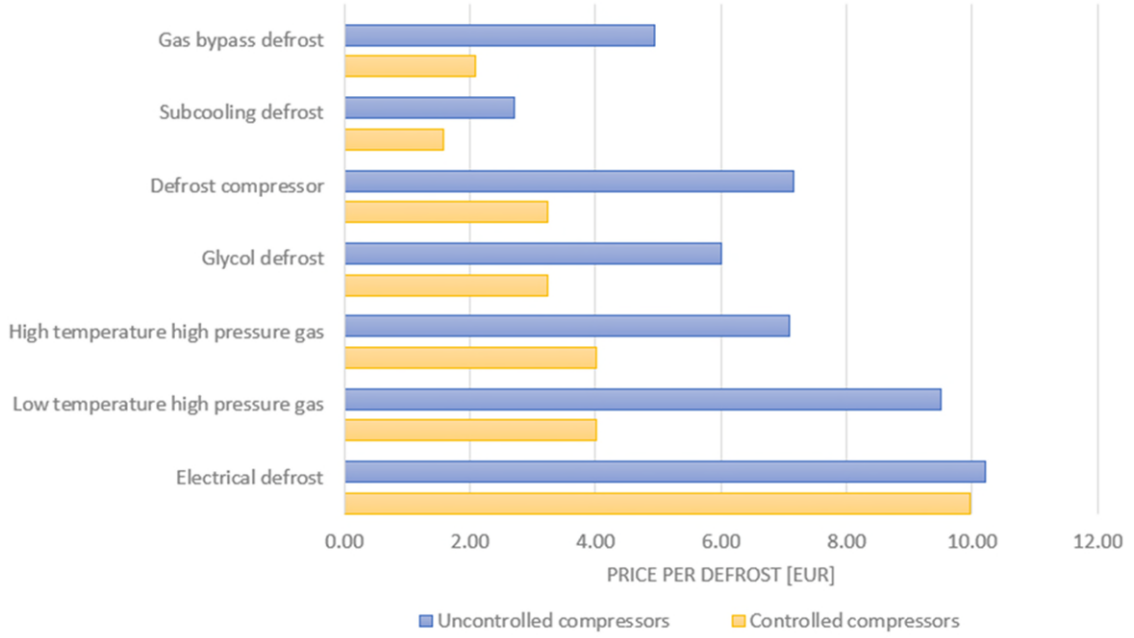

Figure 13: Price comparison of defrost.

With these assumptions glycol defrost turns out to be the cheapest solution. This depends though on the price of electricity and delivered heat.

To verify the defrost, evaluation measurements were taken from two heat pump installations in the field. One installation is in the city of Havneby on the Danish island Rømø in the southern part of Jutland at the West Coast, see Figure 14. The installed heat pump is an air to water heat pump with a nominal capacity of 600kW. This heat pump uses cold gas high pressure defrost. The installation consists of one heat pump unit and four horizontal evaporators of equal size with upwards air flow drawn through the coil.

Figure 14: The Havneby installation to the left and the Alborg installation to the right.

The other installation is in city of Aalborg in the northern part of Jutland at the east coast. The installed heat pump is an air to water heat pump with a nominal heating capacity of 1200kW. This installation is double the size of the one in Havneby and uses glycol as defrost method.

In Figure 15, one defrosts cycle is shown for the heat pump in Havneby. The air temperature was around 5°C, and the relative humidity is close to 85%. The capacity before defrosting was measured as 590 kW on average which was very close to the simulated of 589 kW. The heating COP for the installation was measured as 3.01 on average before defrosting where the simulations calculated 3.27. The explanation for this is that the simulated COP did not include fans and auxiliary equipment where the measured one was the system COP i.e., including all electrical usage.

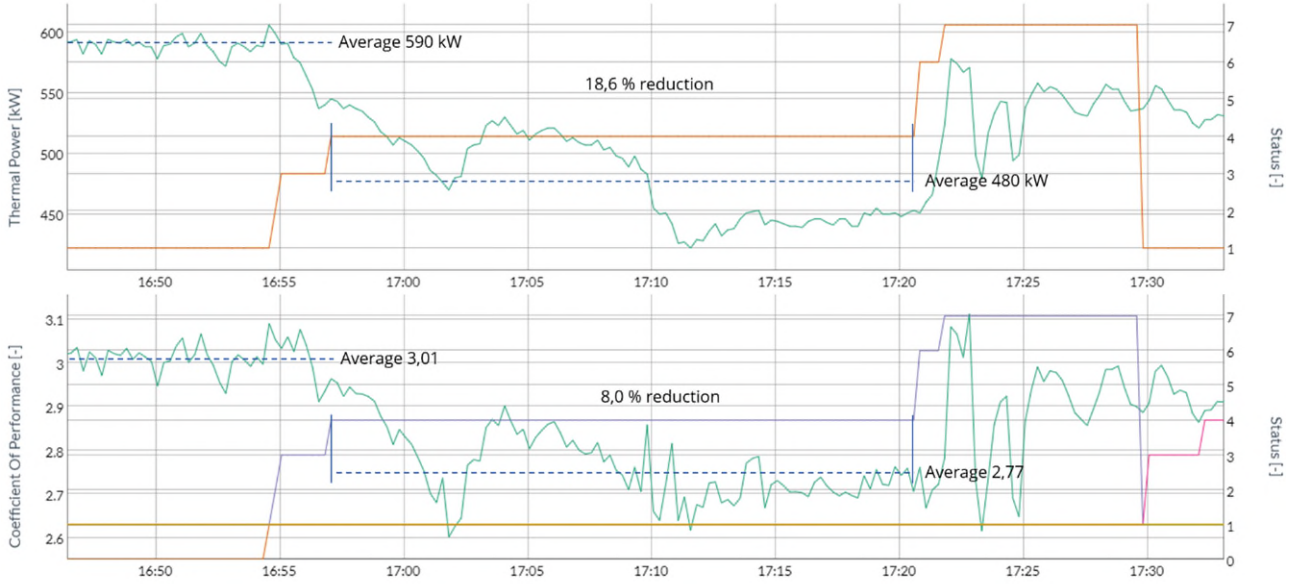

Figure 15: Heating capacity and COP before and during defrost for low temperature high pressure defrost.

The drop in capacity during defrost was measured to be 18.6% calculated from average values through the part of the defrost cycle where the ice was melting. The simulated drop in capacity was calculated to 16.6% which is quite close to the measured one. As seen in Figure 15, the defrost cycle consists of different phases, each with different drops in heating capacity and COP, where the simulated one did not take into consideration the different defrost phases.

The drop in COP was measured to be 8% where the simulated one was 10.7%. It was seen in the measurements that the COP directly after a defrost was measured to be around 3.1 and dropped to 3.01 because of ice accumulation on the coil. When calculating with 3.1 for a clean coil, the simulated and measured drop in COP were very close i.e., measured 10.6% and simulated 10.7%. As seen, the simulations show good agreement with measurements.

When looking at all the phases of the defrosting cycle, the reduction in capacity and COP would be lower than simulated as seen in the graphs since both variables are for most part higher than the average outside the melting phase.

For the installation in Aalborg where the heat pump used glycol defrost, the measurements are shown in Figure 16. Here, there is also a good agreement between the measured and simulated decrease in both capacity and heat production.

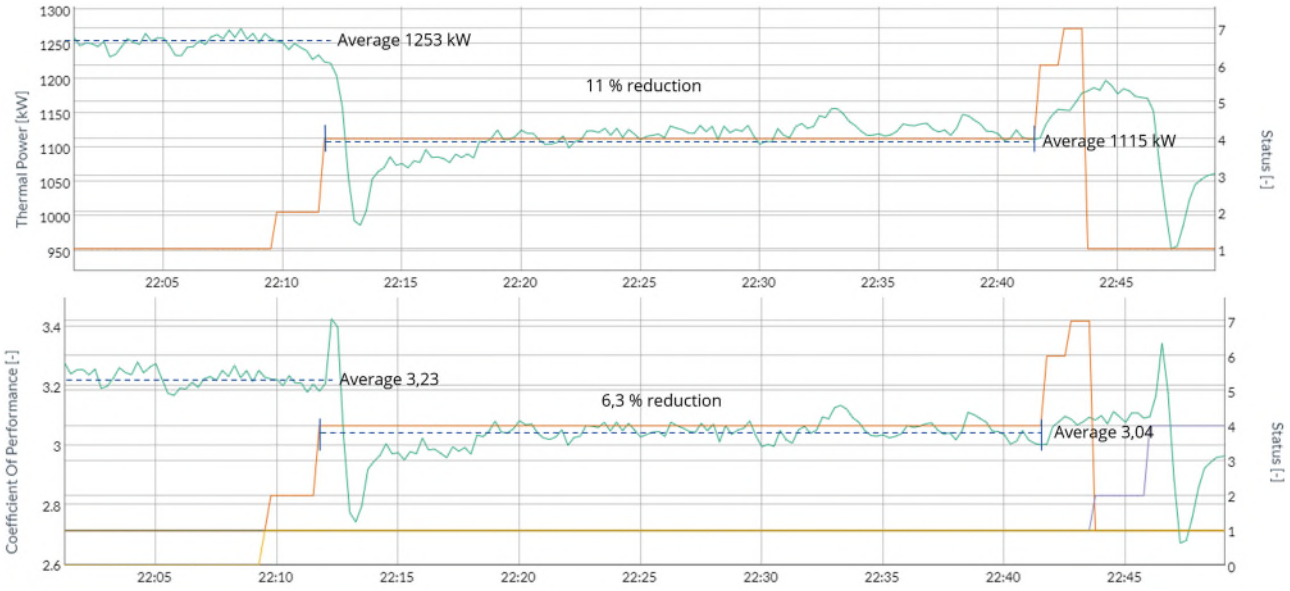

Figure 16: Heating capacity and COP before and during defrost for glycol defrost.

5.1.3.1 Defrost Model

5.1.3.1.1 Model description

In this project, the foundation for a defrost model which can be used for prediction of defrost time of an air-source evaporator is laid. The model aims at defrosting with hot gas (sensible heat) but can be extended to multiple different scenarios. In this model, the defrost process is divided into five separate stages namely pre-heating, melting, melting with air gap, evaporation of residual water layer and dry heating as shown in Figure 17. The model switches between different stages based on trigger conditions, and defrosting completes when the last element enters the dry heating stage. Since the hot gas defrost process is a very complex phenomenon involving several forms of heat and mass transfer mechanisms, this simplification and subdivision is necessary to develop a practical model which can make predictions within reasonable computational time. 1-D energy equations are applied for the hot gas system and the different interfaces. Electrical resistance analogy is applied to calculate the total heat transfer coefficients (UA) for the different layers. The initial conditions for the defrost including the frost thickness and frost density distribution are obtained from the in-house frosting model which is mentioned in Section 5.1.2.2. The combination of the frosting and defrosting model can effectively deal with non-uniform frost formation in the evaporator tubes.

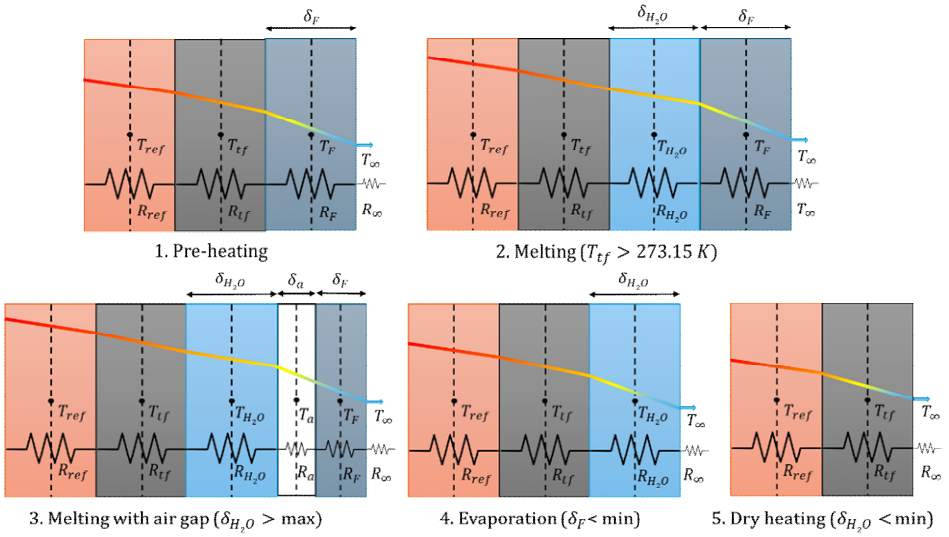

Figure 17: Five stages of defrost process.

5.1.3.1.2 Case study

The evaporator geometry and operating conditions during the normal heat pump cycle is provided as input for the previously described frosting model. The geometrical specifications and input conditions for the evaporator are given in Table 3. The frosting model provides us with the initial conditions of frost layer thickness and frost density present in the evaporator coil at the end of 120 mins. The frost model provides non-uniform distribution of the frost in the different tubes of the coil, and the defrost model is also equipped to deal with this non-uniform frost distribution. The energy equations are solved for the different layers and interfaces in Figure 17, and we get the defrost time required to remove the accumulated frost. The results of the defrost code are explained in the subsequent section.

Table 3: Case study for defrosting.

Tube length	**No. of tubes**	**Frost conditions**	**Gas discharge temperature**	**Discharge pressure**	**Ambient temperature**	**RH**
2.13 m	12	From frost model	110°C	85 bar	5°C	100%

5.1.3.1.3 Results and discussion

Figure 18 left shows the temperature distribution of the hot gas along the total length of the tubes. The hot gas enters from the discharge at 110°C, while the frost is at a temperature of -10°C. As the defrosting progresses, the temperature drops along the length of the tubes also decreases. The total time taken to defrost the tubes is around 161 s. From Figure 18 right, we can see that the elements further in the tube from the hot gas take longer time to defrost as expected. The defrost model can predict the defrost times at different tubes in the evaporator coil. The frost distribution (in terms of tube frost blockage percentage) in the 12 tubes of the evaporator coil at different times in the defrost process are shown in Figure 19. Using the model, we can accurately predict the uneven melting of frost in the different tubes.

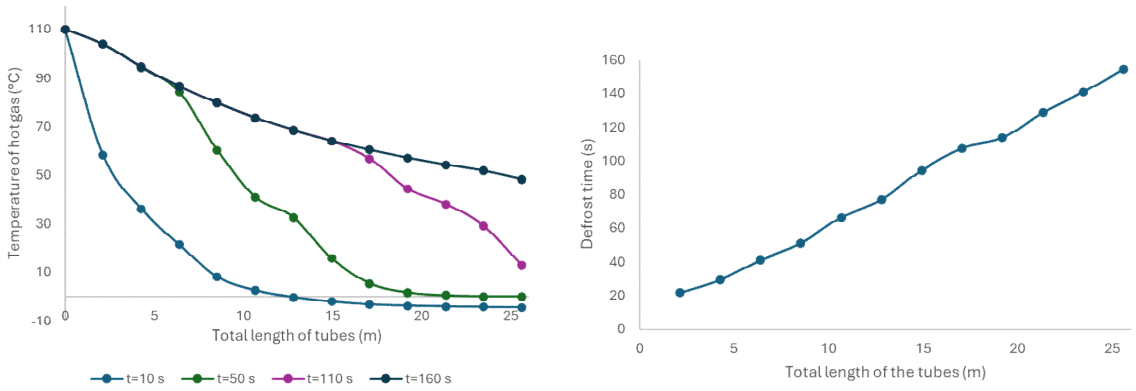

Figure 18: Temperature of the gas across the tube length (left), Defrost times across the tube length in one coil (right).

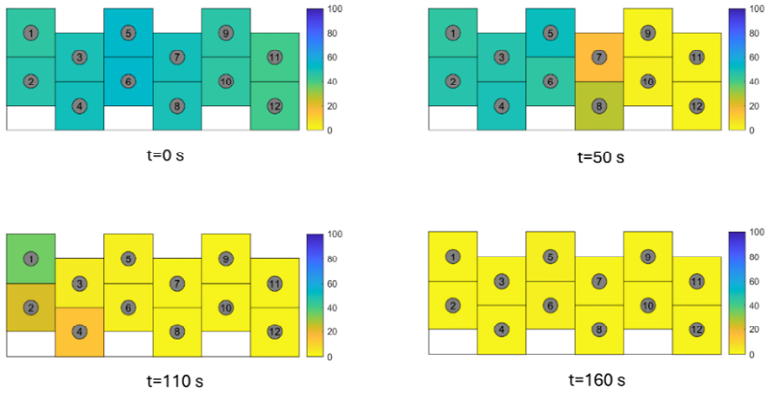

Figure 19: Defrost process in evaporator tubes and fins. Frost blockage (%) distribution at different time steps.

5.1.3.1.4 Conclusions

As a part of this project, a CFD-assisted numerical model is developed to study the frosting behaviour of a V-shape multi circuit evaporator which can be a component of a CO_2 heat pump. The effect of uneven air flow distribution among the circuits of the evaporator on the frost formation non-uniformity has been investigated. Additionally, a generic defrost model was developed by which the defrost time and frost melting phenomenon can be predicted for uneven frosting in the evaporator tubes. The frost growth model can complement the defrost model providing initial frost distribution. The two models together can provide a complete predictive solution to the frosting problem seen in air source heat pumps in cold climates.

5.1.4 Evaporator air circulation

5.1.4.1 Introduction

The evaporator is the largest component in an air source heat pump and constitutes a considerable portion of the investment. It is therefore essential to ensure that the evaporator performs at its highest capacity. The goal of this research activity is to use CFD to study the air circulation around the evaporator to shed light on two main aspects. Firstly, cold air re-circulation into the heat exchanger coils can decrease the inlet air temperature and hence the capacity of the evaporator. An attempt must be made to avoid such a situation. The presence of side wind and buildings particularly makes it important to understand the air flow around the evaporator as these can interfere with the fan-induced flow of cold air out of the evaporator. Secondly, when the heat pump is installed in residential areas, cold air can impact the comfort of residents living in the neighborhood. It is

therefore important to have an estimate of how far the cooling effect is sensed in the surrounding. The present report summarizes research on cold air circulation in the CO2Mix4Heat project. To avoid prolongation, the report contains the most important findings. Complete details are included in an internal report made available to the project partners.

5.1.4.2 Methodology

Commercial software StarCCM+ is used for the CFD simulations in this part of the project. To evaluate the numerical model, to select the appropriate domain size and boundary conditions, and to do some parametric studies, we started this study with a CFD simulation of a one-unit evaporator. The geometry of the one-unit evaporator is given in Figure 20. The four-unit evaporator that was studied later consists of four of the same units.

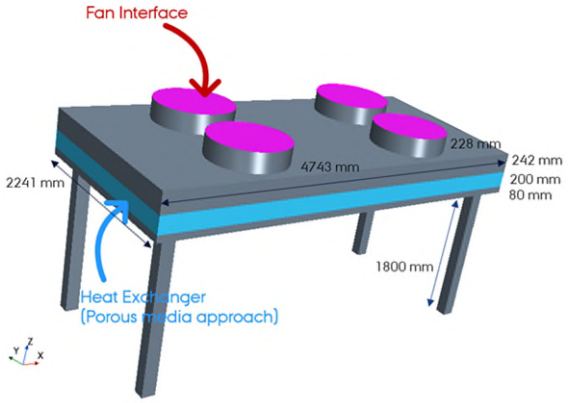

Figure 20: geometry of one-unit evaporator.

The size of the computational domain is selected based on the study done by Franke et al. [1]. The power law wind velocity profile is used for the air velocity inlet boundary condition and is obtained as [2]:

$$\frac{U}{U_{10}} = (\frac{z}{10})^{\gamma}$$

where U is the wind speed at height z (in meters), and U_{10} is the known wind speed at a reference height of 10 m. The exponent is an empirically derived coefficient and is selected to be 0.2. The wind profile of the atmospheric boundary layer (surface to around 2000 meters) is generally logarithmic in nature and is best approximated using the log wind profile equation that accounts for surface roughness and atmospheric stability. The wind profile power law relationship is often used as a substitute for the log wind profile when surface roughness or stability information is not available.

Finned tube heat exchangers were modeled based on the porous media transport approach [3]. Viscous and inertial resistances of the porous media required for pressure drop calculations are calculated based on the heat exchanger's pressure drop at the design point of the evaporator. The fan interface method was used to model the evaporator's axial fans [4]. In this method, by using the fan performance curve, the pressure rise through an axial fan is calculated as a function of local flow rates or velocity. Fan swirl is also included in this simulation. A realizable two-layer k-epsilon model [5] is applied for the turbulence closure.

Polyhedral-shaped cells are used to discretize the computational domain. To verify the grid convergence, four sets of meshes with different grid resolutions, ranging from 4.6 to 7.4 million cells, are examined. Wind speed in these cases is 2.3 m/s. Temperature contours at two different planes are compared for these four sets of meshes. There is no remarkable change in temperature contours when we refine the mesh from 5.2 to 7.4 million cells. We also checked the change in size of small-scale vortexes formed near the windward wall of the evaporator (see Figure 21). The size of these vortexes is almost the same in cases with 6.5 and 7.4 million

cells. Based on the mentioned results, we chose the grid with 6.5 million cells for the rest of the simulations. Figure 22 depicts the temperature distribution in the side wind configuration on the selected grid.

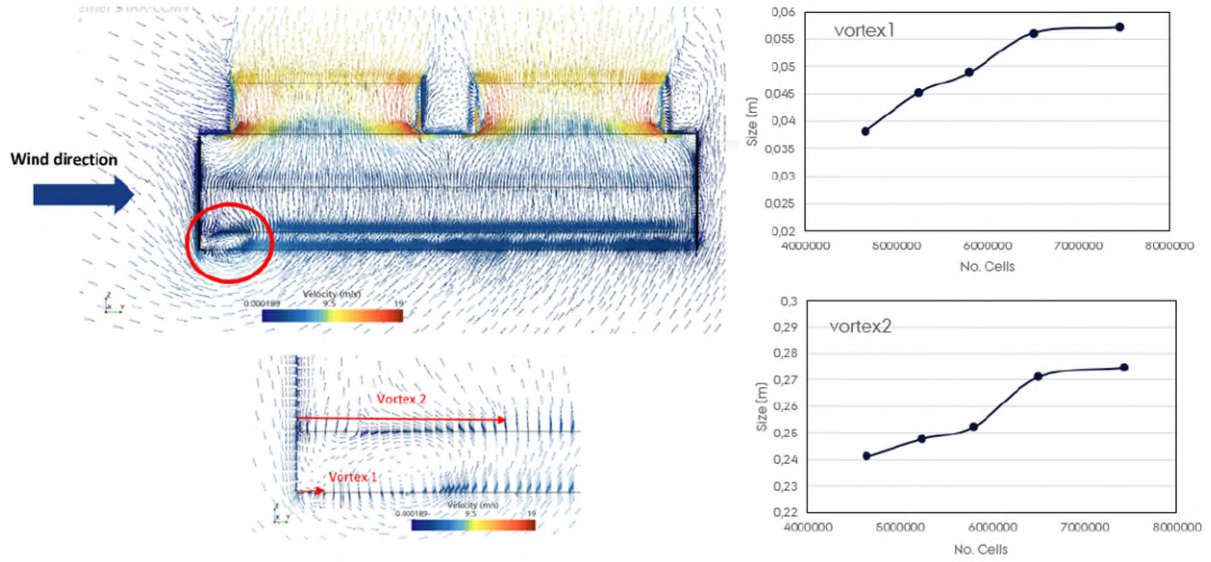

Figure 21: The edge vortex below the evaporator and its size grid independence.

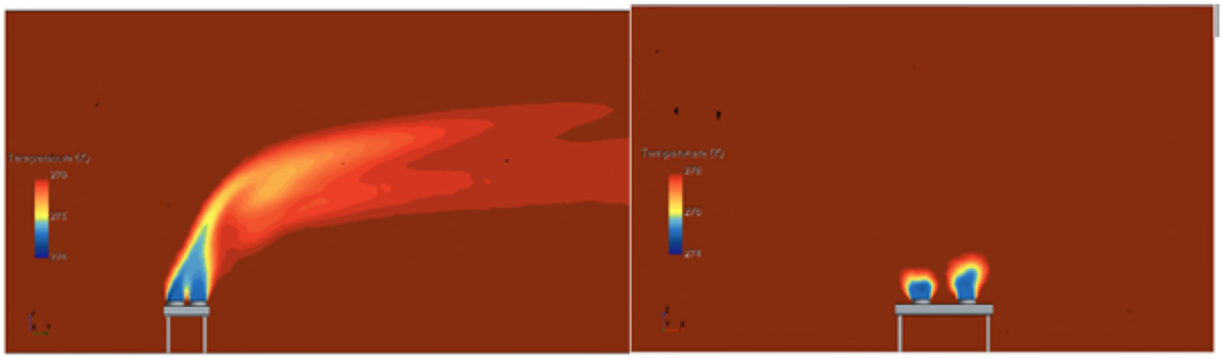

Figure 22: Air temperature due to a side wind of 2.3 m/s shown from side and front views.

5.1.4.3 Results and discussion

5.1.4.3.1 Effect of fan direction on performance

Evaporators with upward and downward flow in fans have been studied regarding the effect of wind speed and wind direction. Each evaporator consists of four units similar to what was shown in the previous section. Wind directions are either parallel to the evaporator arrangement (wind0) or normal to the evaporator arrangement (wind90). In all cases, the ambient temperature is 5°C, and the evaporation temperature is -2°C. Exemplary air temperature contours at different plane sections can be seen in Figure 23 at a wind speed of 7 m/s.

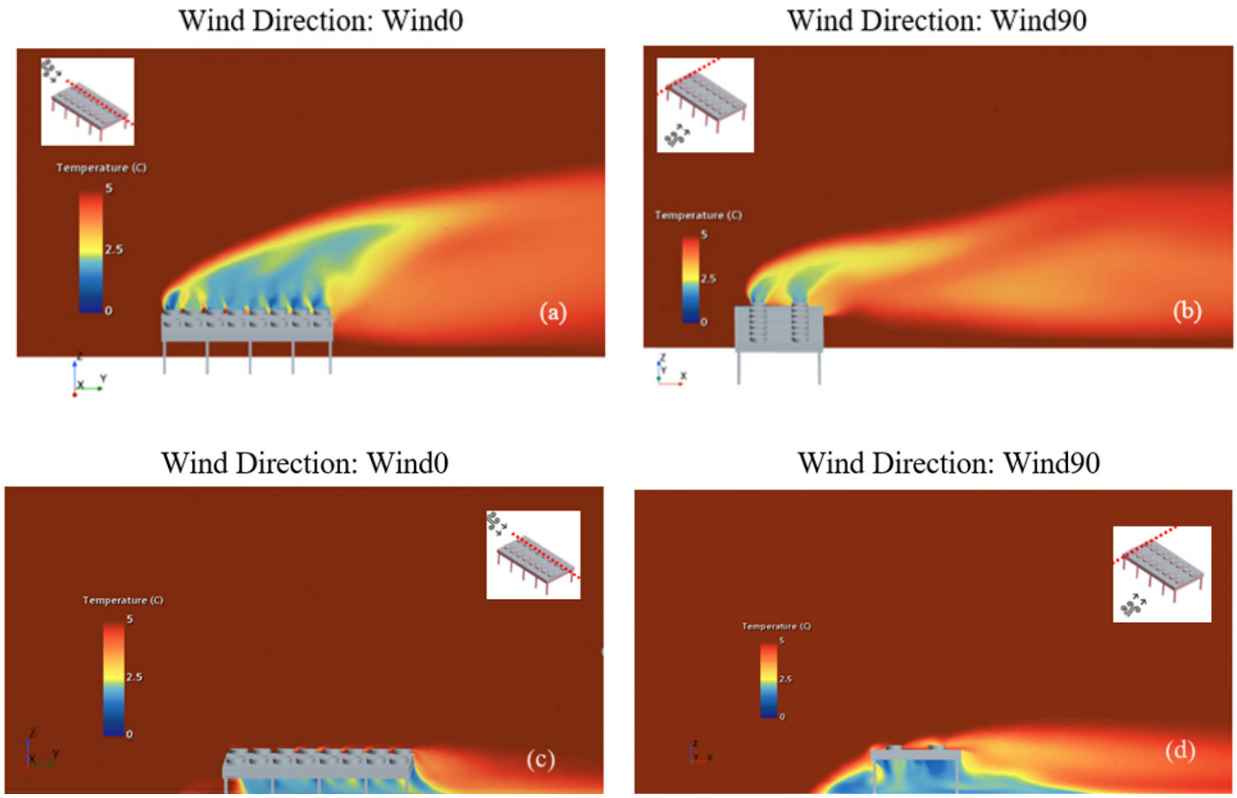

Figure 23: Air flow temperature distribution at wind speed=7 m/s or upward (a,b) and downward (c,d) fan direction.

It is notable that re-circulation of air back into the evaporator can decrease the inlet air temperature and negatively influence the capacity of the evaporator. We systematically studied the effect of fan direction for different wind speeds and angles. The results can be summarized in Figure 24, where the mean inlet temperature (average of all four units) is depicted for both configurations. Overall, there are no significant differences in air temperature between evaporators operating in upward and downward directions. However, the air temperature at the inlet of upward flow evaporators is higher on average than the air temperature at the inlet of downward flow evaporators. In all cases, the inlet temperature drops less than 0.5°C. The only exception is with downward fan direction when the air flow is normal, and the wind speed is low. In this condition, a cold air zone forms upstream of the evaporator which can be partly drawn in by the fans. When the air speed increases, the cold air is simply 'swept' under the evaporator by the strong wind (see Figure 23-c).

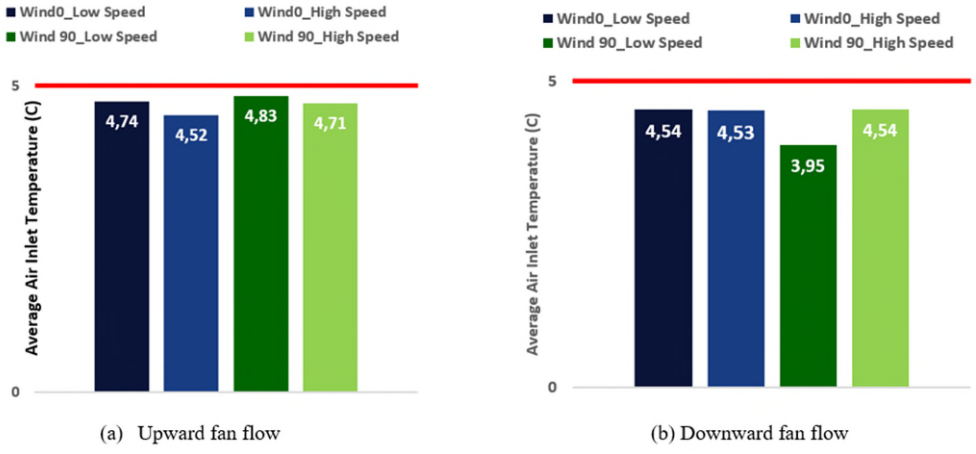

Figure 24: Average air temperature at the inlet of the evaporators. Ambient temperature is 5°C.

5.1.4.3.2 Thermal comfort

To study the possible discomfort due to cold air in the surrounding, upward and downward evaporators are studied in terms of distribution of the cold air. Figure 25 shows an exemplary result in which the area with the temperature 1°C lower than ambient temperature is depicted with blue iso-contours. These cases are for two different wind directions at a speed of 2 m/s; the ambient temperature is, in these cases, 5°C. The figures illustrate how downward flow evaporators affect larger areas both upstream and downstream of the evaporators. The cold air diffuses higher in elevation in upward evaporators than in downward ones, but the latter has a greater impact near the ground.

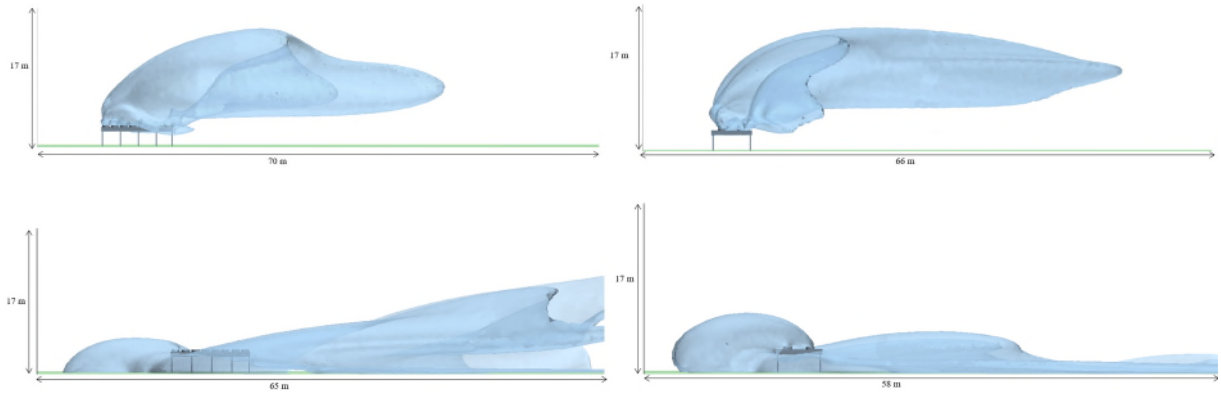

Figure 25: Iso-contours of T = 4°C (ambient temperature - 1°C) for upward and downward fan directions at a wind speed of 2 m/s. Left: wind0 configuration, right: wind90 configuration.

5.1.4.3.3 Effect of nearby buildings and evaporator unit layout

To study the possible effect of nearby buildings, first a 4-unit evaporator (like section 5.1.4.3.2) is placed at different distances (>2 m) from a 6-m-tall building and studied at a wind speed of 7 m/s. No significant reduction in inlet air temperature compared to the previous studies is observed, and the inlet temperature remains above 4.2°C in all cases (ambient temperature 5°C). Note that based on the results of the previous section, the problem is studied for the upward fan direction only.

Following this first study, a much larger evaporator with 24 units of 10 fans was studied at different heights and distances from the building (see Figure 26). Several simulations are run with different evaporator heights (4.6 and 6 m), distances from the building (5 and 10 meter), and wind directions. The largest temperature drop at a certain wind speed was observed when the building is upstream of the evaporator, closer to it and the evaporator has a lower height. This can be visually observed in Figure 27, where the temperature distribution at the inlet plane of the heat exchangers is depicted. Here, on average, a 1.5°C of temperature drop compared to the ambient temperature is observed at the inlet. If the large evaporator is split in two halves, the temperature drop on the downstream half is much more drastic.

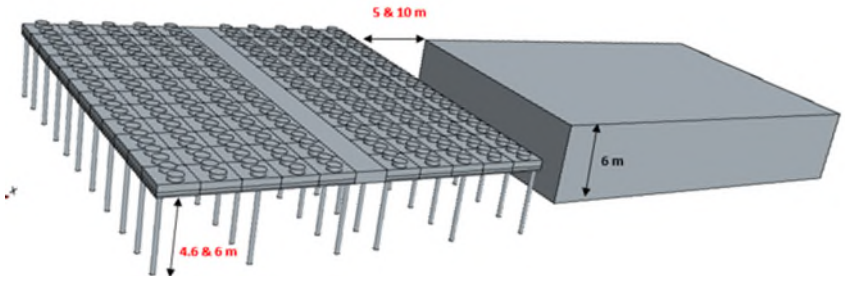

Figure 26: The geometry of the evaporator and nearby building for studying the effect of the nearby building on cold air recirculation around the evaporator.

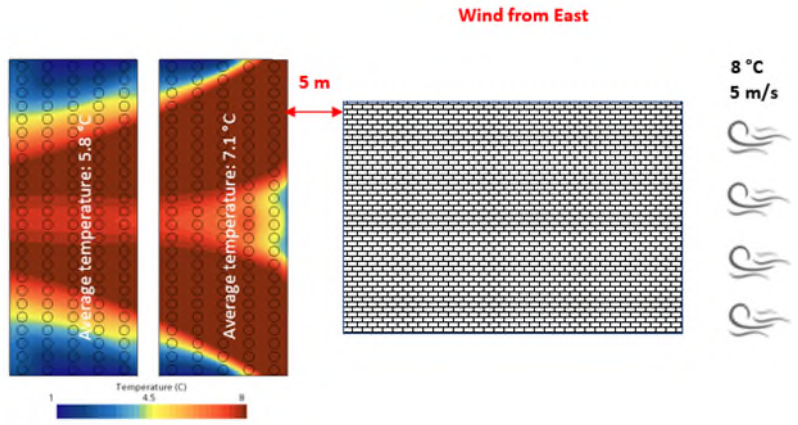

Figure 27: Air temperature distribution at the inlet plane of the evaporator downstream of a 6-m-tall building. The evaporator height is 4.6 m, and the ambient temperature is 8°C. The average air inlet temperature for each half of the evaporator is printed on the figure.

Finally, two different layouts for the large-scale unit shown above are compared. These are the square layout (24×10 fans) and the long layout (48×5 fans). The results are shown in Figure 28 and in Figure 29. Overall, it can be said that the long layout is appropriate for the condition where a dominant direction is known as the inlet temperature can be up to nearly 1°C different for different wind directions.

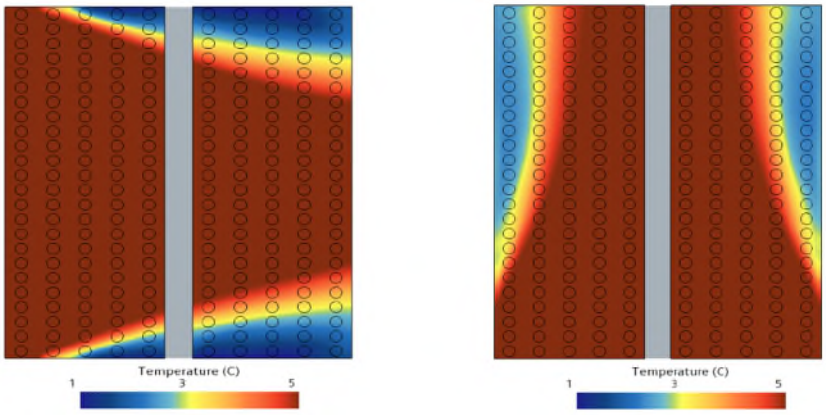

Figure 28: Air temperature distribution at the inlet plane of the evaporator with the square layout. The average inlet temperature is 4.5°C for normal wind direction (left) and 4.4°C for parallel wind direction (right). The ambient temperature is 5°C.

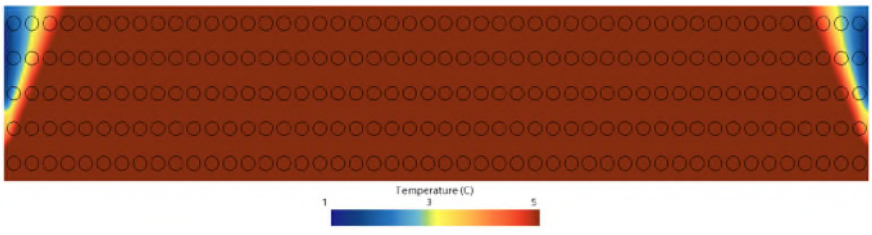

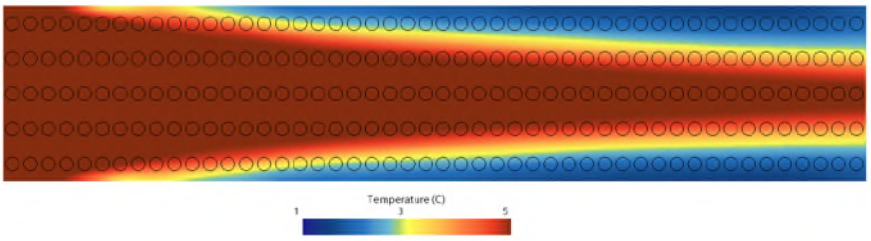

Figure 29: Air temperature distribution at the inlet plane of the evaporator with the long layout. The average inlet temperature is 4.9°C for normal wind direction (top) and 4.0°C for parallel wind direction (bottom). The ambient temperature is 5°C.

5.1.4.4 Conclusions

CFD simulations are used to study the air flow around the evaporators of an air-source heat pump to shed light on the potential loss of capacity due to air re-circulation as well as thermal discomfort in the surrounding. Several cases have been investigated, in which fan direction, wind speed and direction, evaporator height, size and layout as well as the presence of nearby buildings are studied. An upward fan direction is found more suitable based on the analysis of the inlet temperature and the distance by which cold air is felt. With an upward fan direction, a drop in the inlet temperature of more than 0.5-0.6°C can be avoided, in a majority of scenarios at wind speeds of up to 7 m/s. However, special care must be taken when there are large buildings near the evaporator. Moreover, for large evaporators an elongated layout in wind direction should be avoided. CFD simulations can provide an estimate of the air re-circulation patterns and inlet temperatures to avoid the worst scenarios.

5.1.5 Mixtures

5.1.5.1 Introduction

Zeotropic mixtures of natural refrigerants can be considered as attractive working fluid options when there is a temperature glide in the heat sink and/or source of the cycle. Consequently, in the beginning of the CO2Mix4Heat project, special attention has been paid to modeling and optimization of mixture-based heat pumps motivating research on this topic.

While there have been some studies of mixture-based heat pumps in the literature, they mainly address the design point performance, while in real-world, there are multiple scenarios that can lead to part load operation. As a result, in the present research we were particularly interested in answering questions such as: do mixtures show a superior performance over pure working fluids at large temperature glides also when operating at different part load scenarios? Are there any part load scenarios that are favorable for mixture-based heat pumps? Are the optimal mixture compositions the same at both design point and part load operating conditions?

To summarize, the goal of this research activity is to assess the COP enhancement due to the use of mixture refrigerants not only at design point but also at off-design load conditions. Since the results of this activity are published as a journal paper, the present section only features the most important findings.

5.1.5.2 Methodology

In the beginning, design-point optimization was carried out, in which the performance in terms of COP for three different cycle layouts is optimized for a range of different sink/source temperature cases shown based on typical supply and return temperatures in district heating. Figure 30 illustrates the three cycle layouts that are optimized. Note that the condenser is simply illustrated as one component while it can include a subcooler, a condenser, and a desuperheater. Furthermore, in case of a supercritical cycle (which can be optimal for some CO_2/Propane mixtures) it represents a gas cooler. The optimization has focus on performance in terms of COP for the three cycles. From the design point optimization, it is found that the simplest cycle layout – the single

stage with suction gas heat exchanger (SGHX) – has virtually the same performance as the best of the other two cycles. Since this cycle has the simplest layout, the following part load analysis was only performed for this cycle.

It is important to note that the aim of the part-load analysis is not to optimize the heat pump for the highest COP at part load, but rather to assess the same heat pump optimized for full load when operating conditions correspond to part load. In other words, we simulate the steady state of the systems at new values of water temperatures and/or mass flow rate at sink and source. The size of the heat exchangers at full and part load is the same, so the mean temperature difference in the heat exchangers is calculated anew using the estimate of the UA values. Part load operation can occur due to a change in the water return temperature (T_sink.in) or mass flow rate in the condenser (ṁ_water). Obviously, the temperatures and/or mass flow rate at the source side should also be adjusted to meet the reduced heat load. This leads to different scenarios. In the present work, five different part load scenarios are studied which are summarized in Table 4.

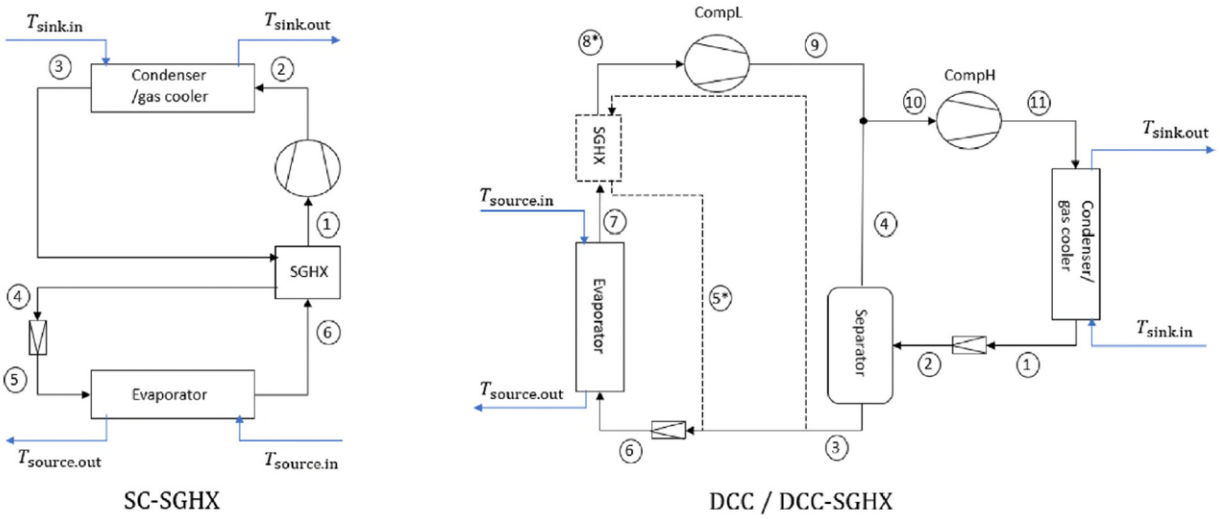

Figure 30: Schematic of the cycles studied.

Table 4: A summary of different part load scenarios.

Scenario	Source		Sink	
	Variable	Fixed	Variable	Fixed
PL1	$T_{source.in}$	$T_{source.out}$, $\dot{m}_{water}$		
PL2	$T_{source.out}$	$T_{source.in}$, $\dot{m}_{water}$	$T_{sink.in}$	$T_{sink.out}$, $\dot{m}_{water}$
PL3	$\dot{m}_{water}$	$T_{source.in}$, $T_{source.out}$		
PL4	$\dot{m}_{water}$	$T_{source.in}$, $T_{source.out}$	$\dot{m}_{water}$	$T_{sink.in}$, $T_{sink.out}$
PL5	$T_{source.in}$	$T_{source.out}$, $\dot{m}_{water}$		

5.1.5.3 Results and discussion

Figure 31 presents the results for the COP of the heat pump at different part load scenarios and five different mixtures. These mixtures are chosen based on the literature and include a CO_2 based zeotropic mixture (CO_2/Propane). For comparison, the results from a pure refrigerant (Propane) are also presented. Note that the weight ratio can be different for each pair of refrigerants. Here, the composition for each mixture is selected based on the design point optimization and equal to the optimal design-point ratio (ODPR). A separate study is conducted for different compositions (not shown here) where, in most cases, a similar trend as in Figure 31. is observed. In Figure 31, all the scenarios are simulated for a heating load of 40% to 100% with 10% increments. It is observed in Figure 31 that in 3 out of 5 scenarios, for all mixtures, performance drops at part load,

but in almost all cases, mixtures deliver higher COPs than the pure refrigerant. Notably, some mixtures are more sensitive to the change of heating load. Conversely, in the scenarios 2 and 4, the trend of the COP with load is either negative or non-monotonic.

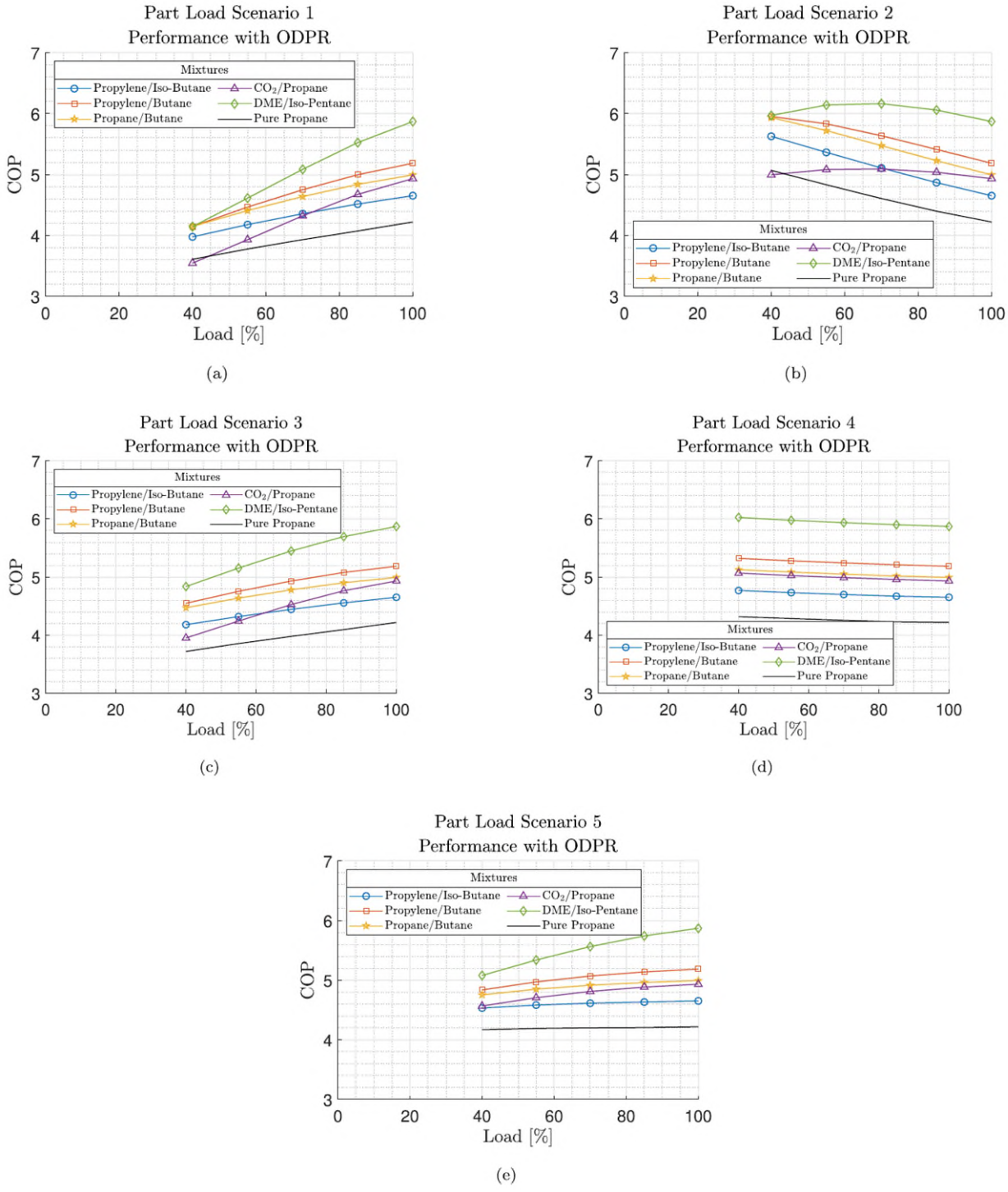

Figure 31: Comparison of mixtures operating at part load. Mixture ratios are ODPR. Part load simulation is based on source temperature of 40°C to 10°C and water (sink) temperature of 40°C to 70°C.

5.1.5.4 Conclusions

The performance of heat pumps with zeotropic mixtures of natural refrigerants is analyzed in full and different part load conditions. The study is focused on five binary mixtures chosen based on previous studies. Based on the design point optimization of different cycles, a single stage cycle with suction gas heat exchanger is selected for further analysis. It is observed that in certain part load scenarios (1, 3 and 5 in Table 4) all mixtures show a decrease in COP when the load is decreased, while in some other scenarios (2 and 4 in Table 4), most mixtures show an increase in COP when the load is decreased. CO_2/Propane and DME/Iso-Pentane in Part Load Scenario 2 are the exceptions to the general behavior. Notably, different mixtures show different sensitivities to part load conditions. Among all mixtures under investigation, DME/Iso-Pentane, while delivering the largest COP in both full and part load cases, is most negatively affected by part load performance. As a result, this mixture can be expected to lose its benefit margin over other candidates at part load.

Overall, the results point towards the fact that the part load performance needs to be taken into account in the design and the selection of a heat pump if the system is expected to perform for a significant portion of its lifetime under such conditions, as the COP can significantly vary with the load and can depend on the adopted scenario. Moreover, for mixture-based heat pumps, the optimal mixture composition may vary with the load.

5.1.5.5 Mechanical subcooling

As mentioned above, the mixture part of the project was diverted to design a so called mechanical subcooling for applications where the return water of the district heating is too high to give the CO2 heat pumps an optimal COP. The dedicated mechanical subcooling (DMS) was developed to use isobutane vapor compression cycle to increase the coefficient of performance (COP) and capacity of the heat pump. A numerical model was developed using Engineering Equation Solver (EES) to simulate the heat pump. Two different integration designs, direct and indirect DMS, were examined and compared to a base case.

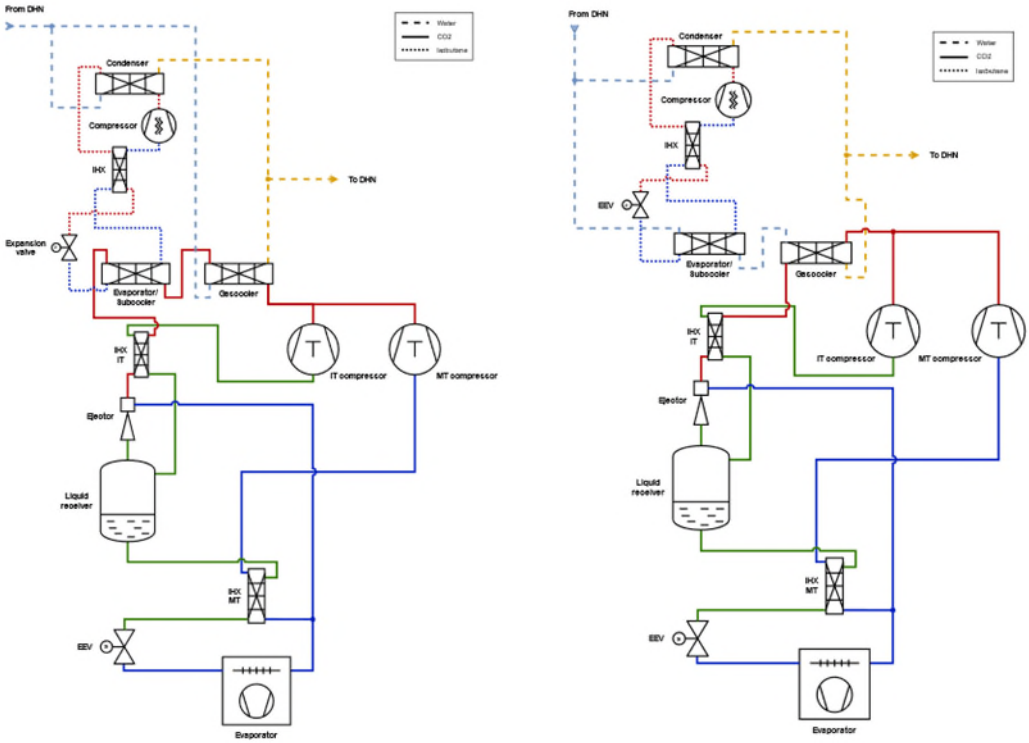

Figure 32: Mechanical subcooling. Direct DMS to the left and indirect to the right

The direct DMS was where the CO2 gas from the gas cooler is directly cooled down by the isobutane heat pump and the indirect is where the water returning from the district heating is cooled down before entering the gas cooler.

The use of direct dedicated mechanical subcooling (DDMS) and indirect dedicated mechanical subcooling (IDMS) on a large-scale air-to-water transcritical CO_2 heat pump, particularly for district heating applications, with high return and supply temperatures. The conditions in which the research was conducted were air temperatures between -12 and 18 °C, return temperatures (from DH) between 40 and 55 °C, and supply temperatures between 60 and 80 °C. The base heat pump, used for comparison of the presented configurations had integrated IT compressors, IHX on IT and MT compressors, as well as a high-pressure ejector. The mechanical subcooling was provided by a vapor compression cycle using isobutane as working fluid.

Results showed that both configurations came with a significant improvement of the COP for the whole system compared to the base heat pump with an average of +14.9% for the DDMS and +9.8% for the IDMS. However, due to its slightly higher performance and smaller components, the DDMS configuration seems more promising. The capacity of the system was also substantially increased by the additional cycle with an average of +22.5% for the DDMS and +24.6% for the IDMS.

5.1.6 CFD solver for two-phase ejectors

5.1.6.1 Introduction

A key component that the project relies on for an enhanced COP is a two-phase high-pressure ejector. A literature survey revealed a limited number of successful attempts at CFD modeling of two-phase ejectors. Moreover, almost all reports in the literature utilized commercial solvers to this end – which is less desired by middle-sized companies due to high license fees. This served as a motivation to explore capabilities of 'open-source' CFD for the problem at hand.

In view of the above, the goal of this research activity is to examine the feasibility of developing a CFD solver for two-phase high-pressure ejectors in the open-source platform OpenFoam.

5.1.6.2 State of the art

Ejectors are substitutes for conventional expansion valves to improve the efficiency and capacity of CO_2 heat pumps. In an ejector, vapor with a pressure and a temperature above the critical point coming from the gas cooler enters the ejector through the motive nozzle and is mixed with the gas-liquid mixture extracted from the evaporator that enters through the suction nozzle (Figure 33). This results in a sudden drop in pressure and temperature of the motive flow. The flow inside the ejector involves a non-equilibrium heat transfer phase change between the two phases, turbulent flow, propagation of shock and compression waves, and a sharp change in the properties of the flow known as flashing. Many features of this complex flow have remained elusive because of the limitations in experiments and complications in numerical studies that are compensated for with a multitude of simplifications.

There are three general approaches in the simulation of two-phase flow within an ejector: mixture, homogenous equilibrium/relaxation, and a two-fluid model. With the knowledge of the shortcomings of the mixture and homogeneous equilibrium/relaxation models used in the majority of the literature [8-12] in resolving local and overall flow parameters we employed a more comprehensive model by employing a Eulerian-Eulerian two-fluid model in the OpenFOAM framework [13]. This approach needs less simplification and can therefore provide a more realistic solution.

The goal of the current work is to provide an open-source tool that can pave the way for resolving local complex phenomena within the CO_2 ejector, improve our understanding of the underlying physics, and predict the overall performance parameters like entrainment ratio with sufficient accuracy to help with design optimization of the CO_2 ejectors. An open-source tool is chosen over the commercial alternatives, owing to the availability of

the source code and transparency of the implemented equations and algorithms which makes it easier to customize the solver, resolve the numerical issues, and improve the outputs.

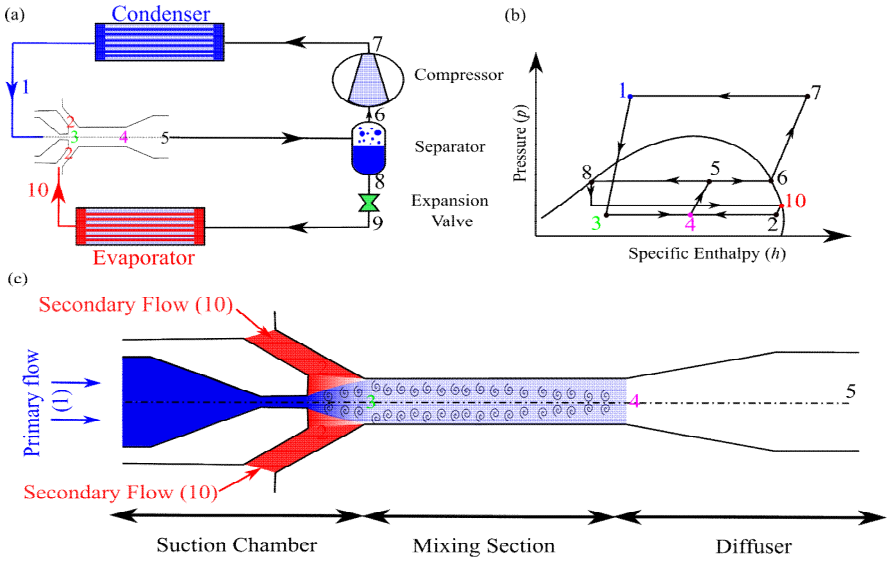

Figure 33: Schematics of (a) the heat pump components and (b) the corresponding thermodynamic CO_2 heat pump cycle. (c) Schematic of CO_2 ejector, where the high-pressure, high-temperature motive flow from the compressor mixes with the high-quality vapor extracted from the evaporator.

5.1.6.3 Governing equations

In this project, a two-fluid Eulerian-Eulerian model is used to simulate the flow field inside the ejector where the governing equations of two phases, liquid (l) and gas (g), are solved separately. The volume fraction α is used to specify how much of each computational cell is occupied by each phase, with the constraint of α_l+α_g=1. Then the conservation of mass momentum and enthalpy, which are the main equations solved by the solver, can be written as:

$$\frac{\partial \alpha_i \rho_i}{\partial t} + \nabla \cdot (\alpha_i \rho_i u_i) = \dot{m}_i$$

$$\frac{\partial (\alpha_i \rho_i u_i)}{\partial t} + \nabla \cdot (\alpha_i \rho_i u_i u_i) = -\alpha_i \nabla p + \nabla \cdot \left\{ \alpha_i \mu_{eff,i} \left[(\nabla u_i + (\nabla u_i)^T - \frac{2}{3} (\nabla \cdot u_i) I \right] \right\} + \alpha_i \rho_i g + \left(\dot{m}_{ij} u_j - \dot{m}_{ji} u_i \right) + \dot{M}_i$$

$$\frac{\partial (\alpha_i \rho_i H_i)}{\partial t} + \nabla \cdot (\alpha_i \rho_i H_i u_i) + \frac{\partial (\alpha_i \rho_i K_i)}{\partial t} + \nabla \cdot (\alpha_i \rho_i K_i i_i) = -\alpha_i \frac{dp}{dt} + \nabla \cdot \alpha_i \mu_{Deff,i} \nabla H_i + \dot{Q}_i$$

where subscript i=l,g represents the phases, and ρ, u, p, H, and K are density, velocity, pressure, enthalpy, and kinetic energy respectively. The interaction of the phases is taken into account through mass ($\dot{m}$), momentum ($\dot{M}$), and heat transfer ($\dot{Q}$) source terms.

5.1.6.4 Validation of the solver

The two-fluid Eulerian-Eulerian approach was chosen after reviewing the existing numerical literature and assessing the solver in multiple benchmarks. In OpenFOAM, the two-fluid Eulerian-Eulerian is implemented in a solver named multiphaseEulerFoam. multiphaseEulerFoam solves the governing equations of each fluid separately and distinguishes the phases using volume fraction. There are a multitude of models implemented in this solver including models for momentum, mass, and heat transfer between the phases, modeling of the dispersed phase, and calculation of the physical properties and thermodynamic states. Therefore, it is not a trivial task to use the solver and gain the desired results. We assessed the solver using multiple benchmarks,

among which two of them are presented in this section: an air ejector and a steam nozzle. The former is a single-phase ejector solver that assesses the capability of the solver in capturing compression waves, and the second helps with finding the best models for resolving the phase change.

5.1.6.4.1 Air ejectors

The flow in an ejector is a single phase and contains strong shock waves similar to what is expected in a CO_2 ejector. We solved this problem using three single-phase solvers and multiphaseEulerFoam. The goal was to validate the implemented numerical method in multiphaseEulerFoam for solving compressible flow without complexities of two-phase flow and mass transfer and compare the results with the other available approaches in OpenFOAM, especially density-based and Rimann-based solvers. Figure 34 shows that multiphaseEulerFoam resolves shock waves with reasonable accuracy compared to the experimental data and other compressible solvers in OpenFOAM. Among the solvers, blastFoam, which is a Riemann-based solver, gives the best results as it smears the shocks less. Therefore, it could be considered a potential approach to substitute the current compressible solver of multiphaseEulerFoam, and improvement in future projects.

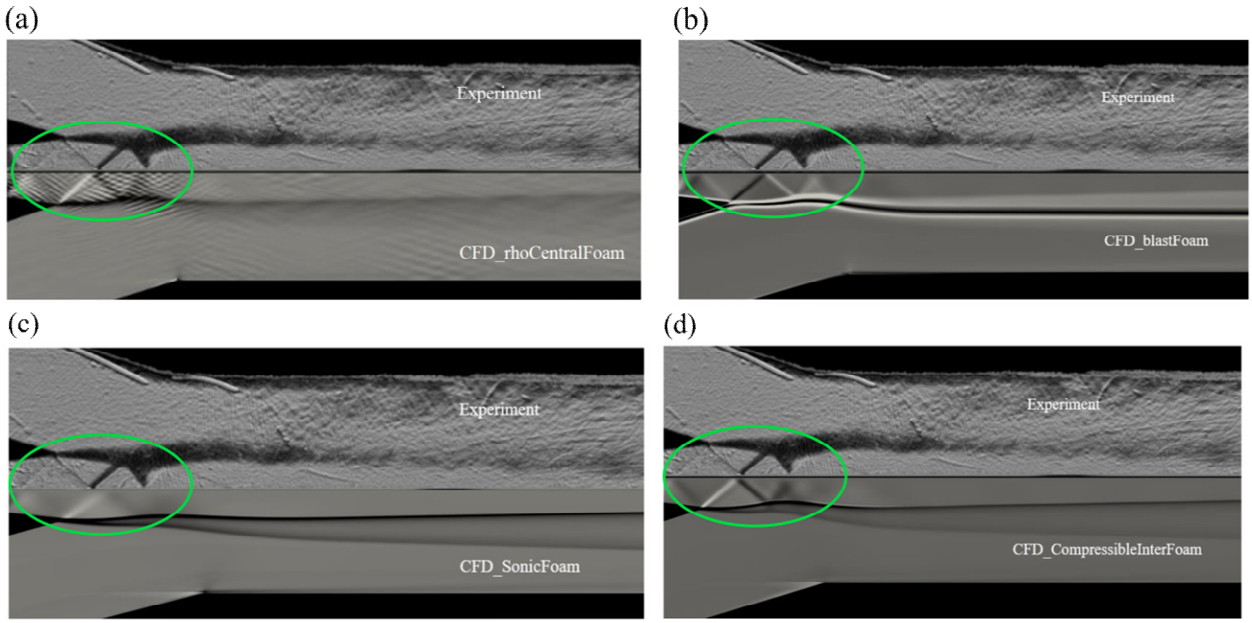

Figure 34: Comparison of different compressible solvers in the simulation of an air-ejector with the experimental results: (a) Density-based, (b) Riemann-based, (c) Pressure-based, single-phase, (d) Pressure-based two-phase Eulerian-Eulerian solvers.

5.1.6.4.2 Steam nozzle

Air ejector case showed that multiphaseEulerFoam can capture the shock waves. Then steam ejector can be used to assess the solver in resolving momentum, mass, and heat exchanges between the two phases. Here, Brookhaven National Lab (BNL) experimental results [14] of liquid water evaporation in a converging-diverging nozzle are used for validation of the solver. We have validated the solver with multiple BNL cases that gave different pressures and temperatures at the inlet and outlet, among which, BNL 309 is numerically the most challenging one. Figure 35 shows the pressure and gas volume fraction in the nozzle. The phase change starts around the throat, where the pressure drops substantially and continues in the diverging part of the channel. The average volume fraction compared with the experiment report and one recent numerical paper [15] shows that the solver well predicts the phase change along the nozzle, see Figure 36.

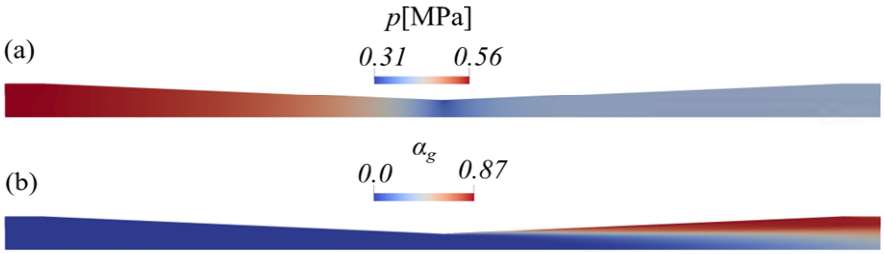

Figure 35: (a) Pressure and (b) gas volume fraction field of BNL309.

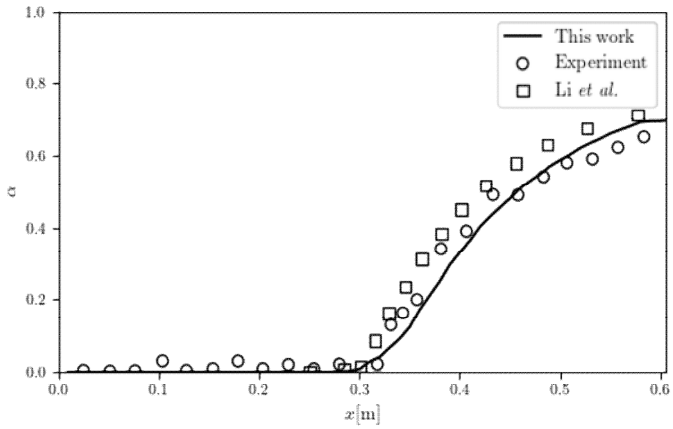

Figure 36: Comparison of the average volume fraction along the nozzle with experimental results of [14] and numerical results of [15].

5.1.6.4.3 Nakagawa nozzle

A correct prediction of the flow field and phase change in a CO_2 ejector requires the real properties which are not included in the original OpenFOAM solver. We imported the properties from the REFPROP library and conducted a series of tests to ensure that the solver can calculate the properties in different states, especially close to the critical point which is the main challenge. The Nakagawa nozzle [16] is used as a standard benchmark to validate the results. Figure 37 shows that the pressure along the nozzle axis is captured accurately.

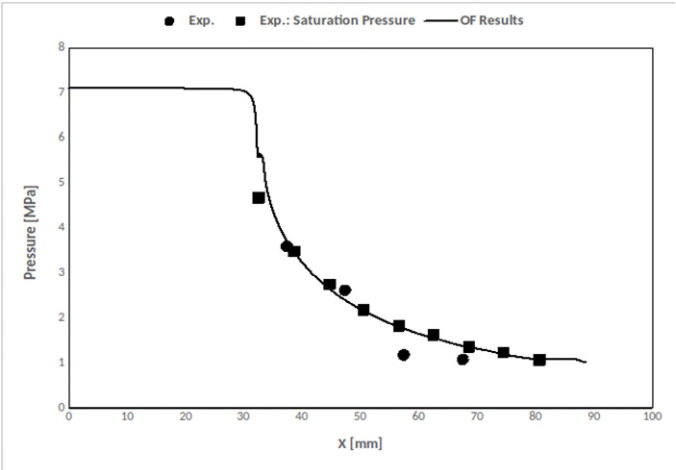

Figure 37: Comparison of the pressure along the axis in the Nakagawa Nozzle with the experimental results [16].

5.1.6.5 Conclusions

Different solvers available in the OpenFoam platform have been customized and systematically studied to explore the possibilities for modeling a two-phase ejector. Special focus was placed on Euler-Euler solvers which in view of the literature could be suitable candidates for the off-critical motive flow conditions where non-equilibrium conditions can challenge less-sophisticated types of solvers. In order to systematically investigate the performance of the solvers for different physical phenomena (shock waves, flashing, turbulence, non-ideal fluid), the solution was assessed for different test cases consisting of air-ejectors, steam nozzles, and CO_2 nozzle. Overall, the results show that a solver based on the multiphaseEulerFoam solver can be a promising choice for simulation of two-phase HP ejectors as it satisfactorily captures different physical phenomena in different test cases.

References

[1] J. Franke, A. Hellsten, K. Schlunzen, B. Carissimo, Best practice guideline for the cfd simulation of flows in the urban environment-a summary, in: 11th Conference on Harmonisation within Atmospheric Dispersion Modelling for Regulatory Purposes, Cambridge, UK, July 2007.

[2] J. D. Holmes, Wind loading of structures, CRC press, 2007.

[3] K. Hooman, H. Gurgenci, Porous medium modeling of air-cooled condensers, Transport in Porous Media 84 (2) (2010) 257–273.

[4] User Guide, Starccm+ version 2020.1, SIEMENS simcenter (2020).

[5] T.-H. Shih, W. W. Liou, A. Shabbir, Z. Yang, J. Zhu, A new k-epsilon eddy viscosity model for high reynolds number turbulent flows: Model development and validation, Tech. rep. (1994).

[6] W. He, D. Han, C. Yue, W. Pu, Y. Dai, Mechanism of the air temperature rise at the forced draught fan inlets in an air-cooled steam condenser, Applied thermal engineering 71 (1) (2014) 355–363.

[7] F. Marincowitz, M. Owen, J. Muiyser, Experimental investigation of the effect of perimeter windscreens on air-cooled condenser fan performance, Applied Thermal Engineering 163 (2019) 114395.

[8] F. Giacomelli, F. Mazzelli, and A. Milazzo. A novel CFD approach for the computation of r744 flashing nozzles in compressible and metastable conditions. Energy, 162:1092–1105, 2018.

[9] J.P. Janet, Y. Liao, and D. Lucas.Heterogeneous nucleation in CFD simulation of flashing flows in converging–diverging nozzles. Int. J. Multiph. Flow, 74:106–117, 2015.

[10] Y. Liao and D. Lucas. 3D CFD simulation of flashing flows in a converging-diverging nozzle. Nucl. Eng. Des., 292:149–163, 2015.

[11] K.E. Ringstad, Y. Allouche, P. Gullo, A. Ervik, K. Banasiak, and A. Hafner. A detailed review on two-phase ejector flow modeling. Therm. Sci. Eng. Prog., 20:100647, 2020.

[12] M. Yazdani, A.A. Alahyari, and T.D. Radcliff. Numerical modeling of two-phase supersonic ejectors for work-recovery applications. Int. J. Heat Mass Transf., 55(21–22):5744–5753, 2012.

[13] H. G. Weller, G. Tabor, H. Jasak, and C. Fureby. A tensorial approach to computational continuum mechanics using object-oriented techniques. Comp. Phys., 12(6):620–631, 1998.

[14] N. Abuaf, B J.C. Wu, G A Zimmer, and P Saha. Study of nonequilibrium flashing of water in a converging-diverging nozzle. volume 1: experimental. 6 1981.

[15] J. Li, Y. Liao, P. Zhou, D. Lucas, and L. Gong. Numerical simulation of flashing flows in a converging–diverging nozzle with interfacial area transport equation. Processes, 11(8):2365, 2023.

[16] M. Nakagawa, M.S. Berana, and A. Kishine. Supersonic two-phase flow of CO2 through converging–diverging nozzles for the ejector refrigeration cycle. Int. J. Ref., 32(6):1195–1202, September 2009.

5.2 Functional analyses – WP05

A test setup was built based on the PI diagram shown in Figure 2. The installed test system is shown in Figure 38. a) in Figure 38 is the part in Figure 2 market as the heat pump unit, and b) is the evaporator 1 and 2 in the PI diagram in Figure 2.

Figure 38: a) Test heat pump rig and b) evaporator in the climate chamber.

This test setup was placed in a climate chamber at Technological Institute in Aarhus and the placement of the evaporator in the climate chamber can be seen in Figure 39. The coil sections are market on in the picture. The coil section C1-1 had the same circuiting on all seven sections of the coil with 36 passes where the last passes were facing the air inlet to have the highest air temperature to supply superheat. For coil C1-2 the passes were distributed unevenly with 34 passes for the three top coil sections, 36 passes in the middle section and, 38 in the three bottom sections. This was done to compensate for the air maldistribution and to try to even out the refrigerant distribution through the coil. For the last two coils C2-1 and C2-2 the passes were the same as for C1-1 but just with two expansion valves instead of one. One expansion valve was used for the three top coil sections and then another expansion valve for the bottom four coil sections. This was done to try to have better control of the refrigerant flow through the coil.

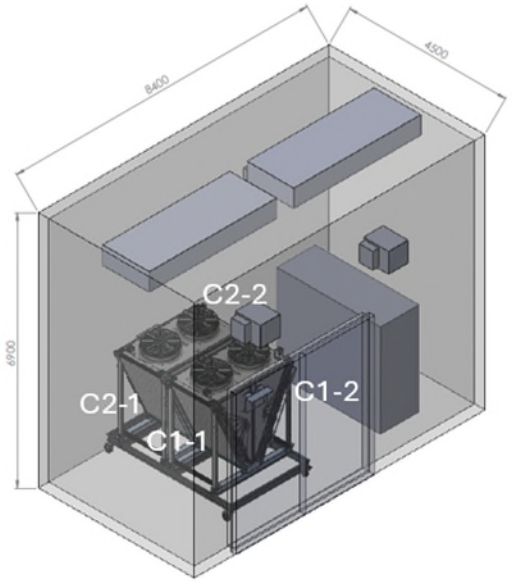

Figure 39: The heat pump evaporator in the climate chamber.

27 tests were done to investigate the air distribution, defrost, coil configuration, and general concept analyses.

Initially, tests were conducted to investigate the control of the unit and investigate defrost. They showed that there were some issues with the air distribution and with the distribution of liquid refrigerant into the coil. As can be seen from Figure 40, the icing up of the end of the evaporator, where the refrigerant changes direction and runs through the coil again, is a good indicator of the different loads on the coil sections and indicates the difference in superheat in each section. There are 7 sections in the coil which are market 7 from the bottom and up to 1 at the top.

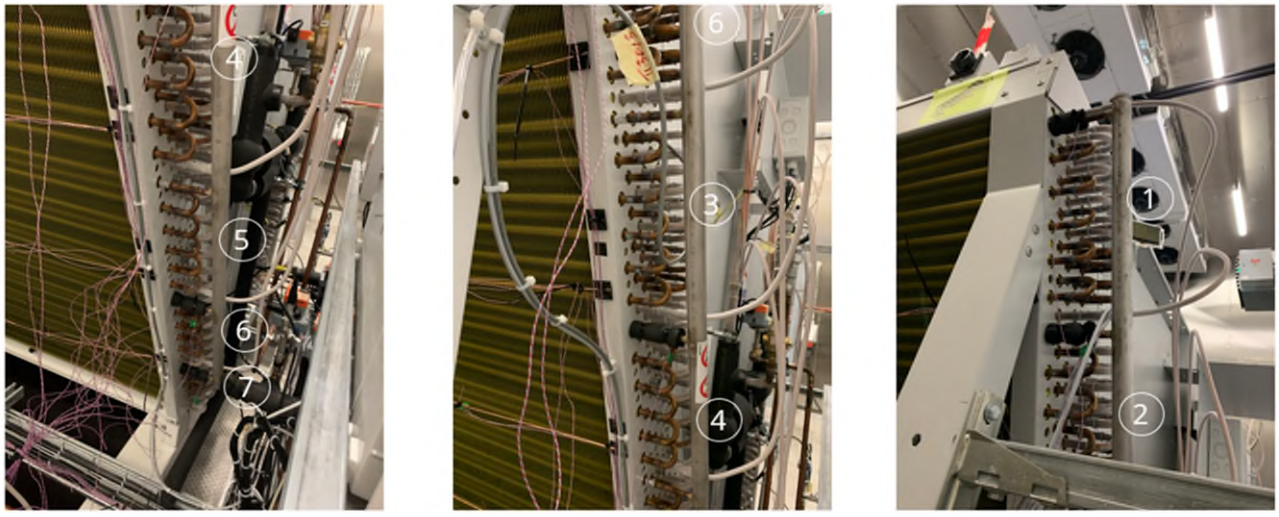

Figure 40: The ice distribution on coil 1.1.

When analysing the pictures, it is seen that the section at the bottom is the one that has the most ice on the outlet of the refrigerant circuit which indicates that it receives the most refrigerant and in fact controls the superheat of all the coil since the coil just has one expansion valve. There are two factors that can cause this, and one is the uneven refrigeration distribution in the coil, and the other is an uneven distribution on the air side.

In Figure 41, the measurements of the refrigerant leaving each section of the coil are shown together with the saturated suction temperature. The difference is the superheat from each coil section. When looking at the superheat signal from each row depictured in Figure 41, it becomes clear that the lowest section number 7 controls the superheat followed by section 6. This can be seen as the distance between the temperatures out of the coils and the saturated suction temperature where the temperature on section 7 falls to the saturated suction temperature indicating that a liquid refrigerant leaves the section. This is in good agreement with the simulations done in the research part.

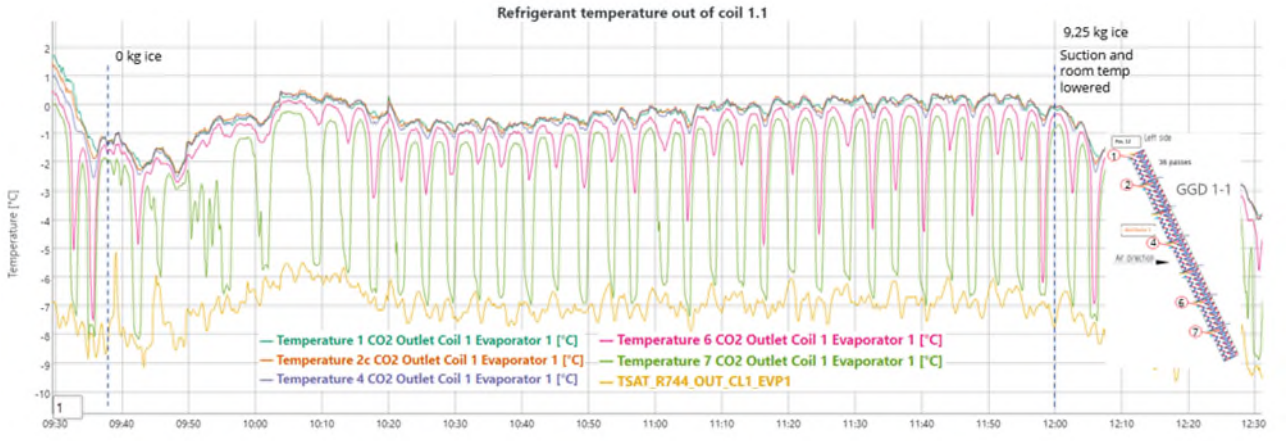

Figure 41: Temperature on the refrigerant leaving different sections of the coil.

By getting liquid into the suction line from section 7, the superheat drops rapidly, and then the expansion valve closes to bring the superheat up again.

From the air side there can be two reasons for an uneven load distribution that can have this influence on the expansion valve. One is the air temperature, and the other is the air flow. Air temperature measurements were done that showed that the air temperatures into the coil were even, so the temperature was not the problem. The next measurements were air speed measurements done with a handheld sensor over the coil surface. These are shown in Figure 42.

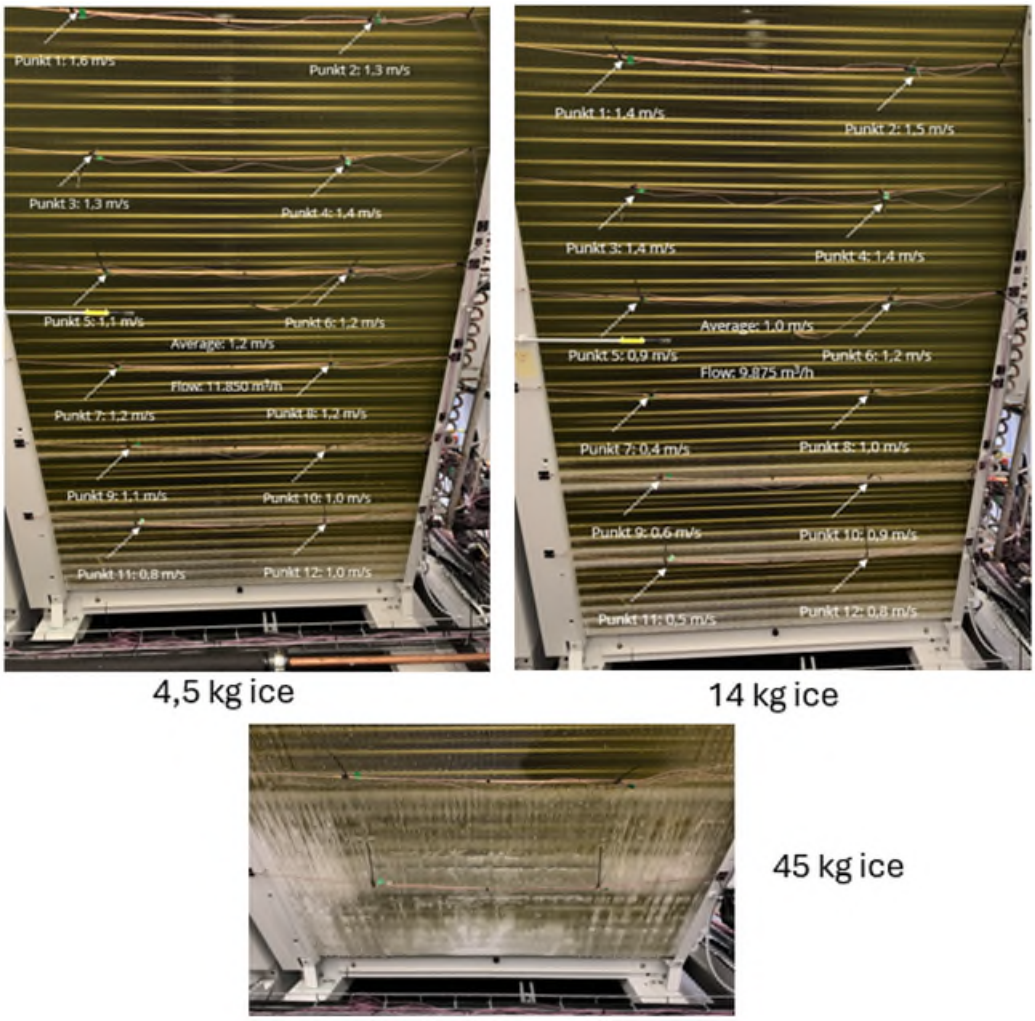

Figure 42: Air speed measurements on coil 1.1 at different ice up rate.

These measurements show that the lowest air flow is in the bottom and highest in the top. The lowest flow gives the lowest capacity from the air, and for the same refrigerant flow to the circuits, the superheat drops, and liquid leaves occasionally the lowest sections 6 and 7. This leads to ice buildup on the coil surface where the air flows into the coil as seen in the pictures. This has also been verified with simulations done in the research part. At last, these coil sections are blocked with ice. This shows the importance of an even air distribution into the coil. To improve this, an air hood was produced by Guentner and installed at DTI. The measurements done for the testing of the air hood are attached to the report as an appendix.

Three different type of coil configuration as described earlier was tested out in the project but the different circuiting and using two expansion valves did not give clear improvements.

As a result of the testing the heat pump design was improved, and a scaled-up version (H300, 300kW) of the heat pump was built and installed outdoor for testing. This unit was after testing transferred to the end user.

Figure 43: H300 heat pump.

Another objective of the project was mixtures where the focus shifted from using mixtures as refrigerant in the heat pump to develop a mechanical subcooling concept to increase the efficiency of CO_2 heat pumps for high return temperatures. Mechanical subcooling consists of using an iso-butane heat pump to bring down the temperature of the return water before entering the CO_2 heat pump. An isobutane heat pump was built and connected to the mixing loops at Technological Institute and tested.

Figure 44: HCI mechanical subcooling unit to the left and installed at Technological Institute at left.

Measurements were used to verify the models made in the research part. The tests showed the estimated improvements from the models.

An initial theoretical investigation of the mixtures was done, and it showed very promising results, if the temperature glide on the source and sink side was above 25°C.

5.3 Functional analyses of CO2 system at district heating site – WP06

To test the heat pump concept at district heating site Harlev district heating was chosen as a field test case. A 600 kW air to water heat pump was installed to produce hot water to the district heating of 70°C supply and

40°C return. The heat pump was installed at a biomass-fired district heating plant in Harlev outside Aarhus, where it was part of the operation together with a straw boiler and some oil boilers at peak load and as backup. The installation can be seen in Figure 45.

Figure 45: 600 kW field test unit in Harlev.

6. Utilisation of project results

Fenagy have used the obtained technological results as the basis for a heat pump product series directed to the district heating sector. They have also paved the way for larger heat pumps using CO2 as refrigerant. The project has been a major factor in Fenagy's growth as a company both on increasing employment and turnover.

Fenagy has also developed their ejector product to large sizes of CO2 heat pumps in the project.

Danfoss have in the project designed and are now producing and selling large sizes high-pressure valves for industrial CO2 applications on the worldwide market. These valves are increasing Danfoss turnover and employment in the industrial valve department.

Gunetner has through the project developed a V-shape evaporator where the air flow into the evaporator is optimized. On the basis of results from the project a new product line of larger sizes of v-coil is being made and marketed to the international market. Here Guentner has increased their turnover and employment.

Vatherus have used the projects results to get a clear understanding of where their strength and weaknesses are.

After the project finished and after Fenagy announced a new product some of their competitors (i.e. Advansor) have designed a similar concept based on the components designed in the project and are competing in the heat pump market.

A European directive called ECO design that is intended to increase the energy efficiency of domestic heat pumps and chillers are in the process of extending their range from 400 kW to 1000 kW and thereby the product developed in the project will be affected. The ECO design as it is built up now considers just space

heating and low temperature radiator heating systems with small temperature differences on the water site. This is not the market CO2 is targeting which is replacing fossil fuel boilers with heat pumps where the supply temperature is from 70 to 90°C and the return temperature is from 30 to 50°C. This will be a problem for CO2 heat pump producers, and we are in discussion with leading technical consultants in the EU on eco-design and energy labeling around how to change the standards to allow for very efficient CO2 solutions. There has also been gathered some CO2 producers of heat pumps to make a common front to push for changes to the standard.

The project results have contributed to a heat pump solution for smaller district heating companies to be able to turn away from fossil fuel boilers to more sustainable solutions to provide heat to their customers.

The project results have been integrated into the heat pump courses at Danish Technological Institute and into the course material at Aarhus university.

Regarding other dissemination activities, an article was written in the International Journal of Refrigeration in 2022 about the use of mixtures in heat pumps.

A presentation of the project was done on a theme day held at Dansk Fjernvarme in 2022. The focus was on defrosting evaporators.

In 2023, a presentation was made on the 8th international symposium on Advances in Refrigeration and Heat Pump Technology conference in Denmark around defrosting in CO_2 heat pumps and the use of mechanical subcooling to boost the efficiency of CO_2 heat pumps for high return temperatures.

A paper was written and presented at the IIR2023 in Macedonia around defrosting in CO_2 heat pumps. Another paper was written and presented at the ICR2023 conference in Paris around mechanical subcooling.

7. Project conclusion and perspective

- *State the conclusions made in the project.*
- *What are the next steps for the developed technology?*
- *Put into perspective how the project results may influence future development*

The project has proven that CO2 can be used for heat pumps for the district heating

8. Appendices

- Add link to relevant documents, publications, home pages etc.